Mineralium Deposita (2023) 58:661–680
https://doi.org/10.1007/s00126-022-01148-6

ARTICLE

Neoformation of exotic copper minerals from gel-like precursors at the Exótica deposit, Chuquicamata, Chile

Frédéric Lambiel[1] · Bernhard Dold[1,2] · Jorge E. Spangenberg[3] · Lluís Fontboté[1]

Received: 30 October 2020 / Accepted: 7 October 2022 / Published online: 16 November 2022

Abstract

At the Exótica deposit, south of the giant porphyry copper deposit of Chuquicamata (Atacama Desert, Chile), Cu-rich groundwater seeped out at several locations in the Exótica open pit (Mina Sur) during sampling in 2009–2011. At their outflows, these solutions formed blueish and greenish copper-bearing gel-like precipitates. These gels contained atacamite and copper sulfate hydroxides such as devilline, spangolite, posnjakite, schulenbergite, and brochantite, which were identified by XRD, SEM, ESEM, and FTIR. The formation of the gel materials was studied under humid and dry conditions during and after maturation and water evaporation. Atacamite was found associated to outflowing saline solutions with pH 5.7, SO_4/Cl weight ratios of 0.42–0.48, SO_4/NO_3 ratios of 0.48–0.50. These solutions are seen as an expression of the the lower aquifer of the Calama basin. Most copper sulfate hydroxides (spangolite, posnjakite, schulenbergite) were associated with slightly acidic freshwaters (pH 6.0 to 6.5, SO_4/Cl ratios of 3.08–4.99, SO_4/NO_3 ratios of 2.52–3.13). In contrast, devilline formed in gels with near neutral to slightly alkaline water (pH 7.2 to 7.8, SO_4/Cl ratio of 8.34, and SO_4/NO_3 ratio of 6.05). Non-copper-bearing precipitates formed by evaporation of the supernatant solutions from the gel. Gypsum precipitated first, then blödite (sodium-magnesium sulfate), and finally halite. Slightly negative sulfur isotope values suggest that the sulfur source in the neoformed gels is primarily the oxidation of sulfides rather than sulfate of sedimentary origin. The studied copper-gel seeps suggest that they might represent a modern precursor of the latest atacamite-brochantite-gypsum mineralization event at Exótica. These data support that the atacamite-brochantite-gypsum mineralization at Exótica is linked to the inflow of Cl-SO_4-dominated groundwater from the lower saline aquifer of the Calama basin into the Chuquicamata-Exótica-Radomiro Tomic complex.

Keywords Atacamite · Brochantite · Posnjakite · Devilline · Supergene · Cu-gel

Introduction

Since 2005, Cu-rich solutions have been observed at several places in the open pit of the Exótica deposit also called Mina Sur (Fig. 1), the "exotic" mineralization south of the giant porphyry copper deposit of Chuquicamata, Atacama Desert, northern Chile. The Exótica mineralization comprises chrysocolla, copper pitch/wad, and the atacamite/brochantite mineral association (Münchmeyer 1996; Pinget 2016; Dold et al. 2022). At the outflow of the Cu-rich solutions, light blue and greenish Cu-bearing precipitates formed semi-solid materials and dried crusts. In the present study, we use the term gel to refer to the semi-solid, copper-rich gel-like materials (Fig. 1). Only a few occurrences of Cu-rich gel-like materials in copper mines or elsewhere have been reported (Moreton 2007; Tumiati et al. 2008; White 2010; Smuda et al. 2014; Majzlan et al. 2018; Majzlan 2020). Gels are defined as polymeric two-phase (liquid and solid) systems (Almdal et al. 1993; Rogovina et al. 2008; Dušek and Dušková-Smrčková 2020). Although these materials have wide technical and chemical applications and potential even in soft robotics (Kuksenok et al. 2014), they have received only marginal interest in geosciences. In contrast, the geochemistry and secondary mineralogy of supergene environments are widely studied (Brimhall et al. 1985; Crane

Editorial handling: F. Tornos

✉ Bernhard Dold
bdold@sumirco.com

[1] Department of Earth and Environmental Sciences, University of Geneva, CH-1205 Geneva, Switzerland

[2] Pontifical Catholic University of Peru (PUCP), San Miguel, PE 15088 Lima, Peru

[3] Institute of Earth Surface Dynamics (IDYST), University of Lausanne, CH-1015 Lausanne, Switzerland

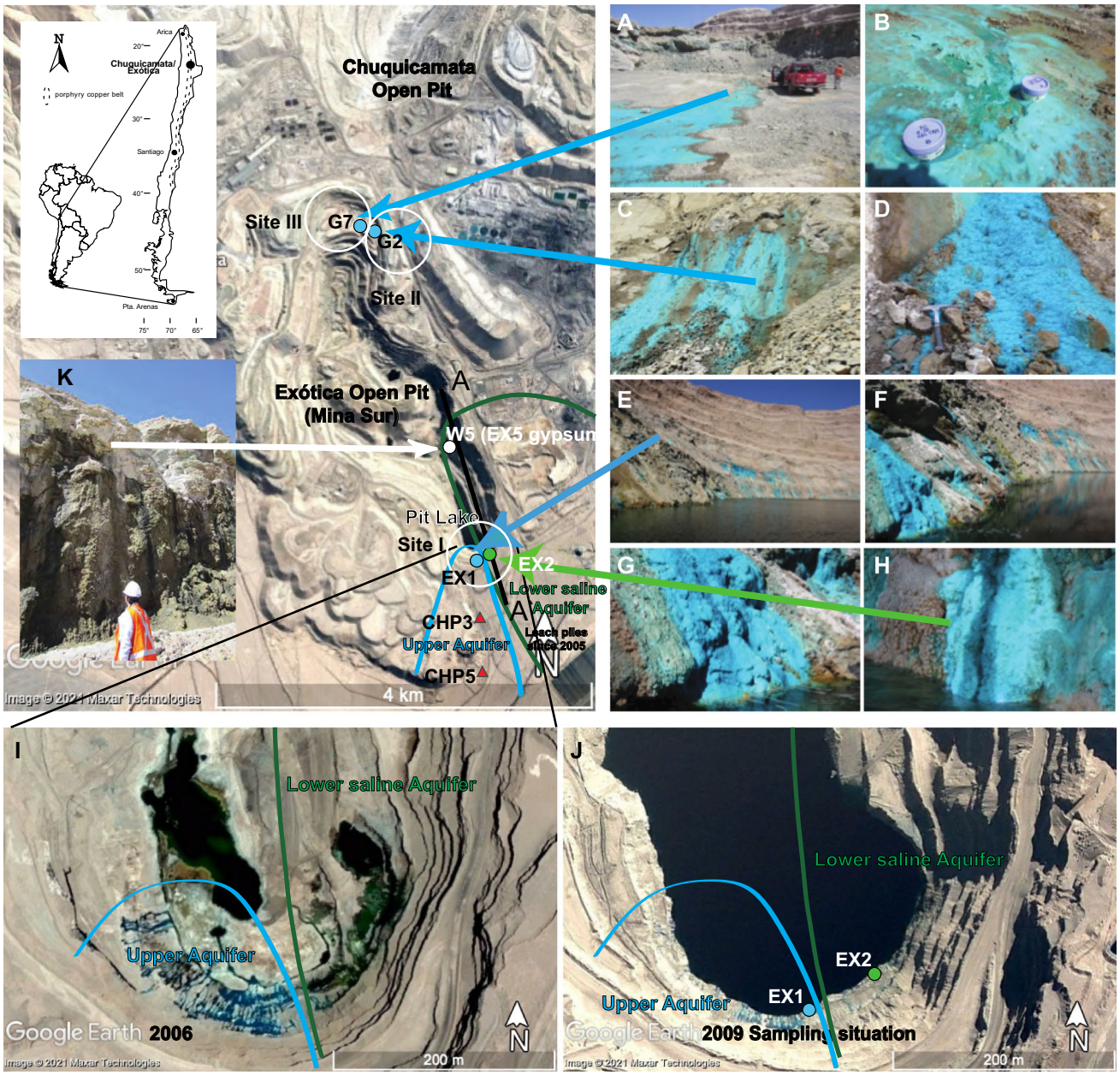

Fig. 1 Appearances of blue to green copper gels in the open pit of Exótica mine, Chuquicamata. **A** View of site III from which the gel samples 7C1, 7C2, and 7B were obtained. **B** Closer view of site III showing the dark green crust of malachite underlying the gels in surficial ponds. **C** and **D** Views of site II from which gel samples 2S and 2 N were collected, respectively. **E** and **F** Gels at site I above the pit lake. **G** Closer view of the site of sampling of gel EX1. **H** Closer view on the atacamite gel mass from which sample EX2 was taken. **I** Google Earth image from 2006 of the southern part of the Exótica open pit (site I). On the left side, the light blue gels (Cu-sulfate hydroxides) from the upper aquifer can be differentiated from the greenish atacamite associated with the lower saline aquifer to the right. **J** Google Earth image from 2009 of the southern part of the Exótica open pit showing the location of samples EX1 and EX2 at the shoreline of the pit lake. **K** Image shows the groundwater outflow (sample W5) in the East wall of the pit, where massive gypsum (sample EX5) precipitates

et al. 2001; Mote et al. 2001; Enders et al. 2006; Sillitoe 2005, Biagioni et al. 2018; Riquelme et al. 2018). The most investigated modern equivalent systems are those associated with the formation of acid mine drainage (AMD) from mine waste (Dold and Fontboté 2001; Graupner et al. 2007; Dold 2014; Nordstrom et al. 2015; Majzlan 2020).

The formation of the Cu-gels in the southernmost part of the Exótica open pit coincides with the end of the mining

operations (Figs. 1E–H) and the cease of groundwater pumping to maintain the pit dry. The relationship between cessation of pumping and gel appearance suggests that the formation of these materials is due to groundwater inflow (Fig. 1). Additionally, further mining of mineralized areas south of the 2011 pit limits confirmed the presence of exotic mineralization in the southern area of the Exótica pit. In the northern part of the Exótica pit (Figs. 1A–D), the gels were associated with water leakage from drilling of blasting holes and other technological/industrial activities. During the sampling campaigns 2009–2011, dissolution and precipitation of copper minerals was observed when the water came into contact with the Exótica mineralization. The question arose as to whether understanding the geochemical processes that led to the formation of the Cu-gels would give insights into the formation of Exótica mineralization. This new knowledge could apply to the supergene processes in the whole Chuquicamata district (Münchmeyer 1996; Ossandón et al. 2001; Pinget 2016). The aim of the present study was to identify the geochemical processes dealing with the formation of the Cu-rich gels in the Exótica open pit and thereby contribute to the understanding of the genesis of the Exótica deposit. We used mineralogical, elemental, and stable isotope data to constrain the processes leading to Cu-gel formation. Additional information was obtained from laboratory experiments with humid and dried gels at different stages of aging. We hypothesize that the formation of the copper gels at Exótica is due to differences in the hydrogeochemical composition of the Cu-gel forming solutions that in turn depend from extent and effect of water–rock interaction processes.

Geological and geochemical background of Chuquicamata-Exótica

The Exótica deposit is mainly hosted by the Fortuna gravels, consisting chiefly of granodiorite clasts derived from the adjacent Fortuna granodiorite (Pinget 2016; Dold et al. 2022). The gravels are deposited along the Exótica Valley heading southwards to the Calama basin. The Calama basin and several other forearc basins were formed during the Late Tertiary (Scheuber et al. 1994; May et al. 2005) in response to the uplift of the Precordillera. The basement of the Calama basin is formed by extensively faulted and brecciated Paleozoic metamorphic rocks, and a Permian to Carboniferous igneous complex (Ossandón et al. 2001; Rivera et al. 2012). The tectono-sedimentary evolution of the Calama basin fill is summarized in May et al. (2005) and Sáez et al. (2012). Sedimentation started in the Eocene with deposition of alluvial braidplain deposits (Calama Formation). From 22 to 10 Ma, ephemeral fluvial sediments were deposited along the Calama basin flanks (Lasana Formation), with a transition to playa sandflats and mudflat deposits (Jalquinche Formation) in the endorheic basin center (May et al. 2005). Late Miocene sedimentation occurred diachronously across the northern Chilean forearc. Regional palustrine carbonate sedimentation occurred in the Calama basin forming the Opache Formation (May et al. 2005; Sáez et al. 2012). The resulting hydrogeological setting in the western Calama basin is mainly characterized by two aquifers. A lower mostly confined aquifer is associated with the Calama Formation and confined in the center by the Jalquinche Formation. An upper phreatic aquifer is associated with the Opache Formation. The moderate to high permeability units sandwiched between low-permeability units form a patchwork of areas with increased water exchange between the two aquifers and areas of low transmissivity where the aquifers are confined. The sedimentary layers terminate westward against the faulted edge of the north-trending basement uplift (Falla Oeste fault system). There, the lower aquifer flows into the upper aquifer and groundwater discharges into local rivers (Jordan et al. 2015). The Fortuna gravels, main host of the Exótica deposit, are considered to be roughly time-equivalent of the Jalquinche, Lasana, and Opache formations (May et al. 2005; Dold et al. 2022).

In the Chuquicamata deposit, a range of green copper sulfates and hydroxide chlorides (i.e., antlerite, brochantite, and atacamite) formed the main oxide ore body (Palache 1939). Additionally, the light blue chrysocolla and the blueish copper sulfate chalcanthite were also found in the oxidation zone of Chuquicamata ore. At Exótica, chrysocolla dominates the mineral assemblage (Münchmeyer 1996; Pinget 2016; Dold et al. 2022) together with a greenish atacamite/brochantite blanket on top. Four main mineralization steps have been identified in Exótica by Dold et al. (2022) and are summarized below:

(1) The exhumation of the porphyry copper sulfide orebody at Chuquicamata during the Andean uplift caused the oxidation and erosion of ~ 900 m of sulfidic mineralization. This step led to the formation of acid rock drainage (ARD) with fluids flowing southward into the Calama basin through the Exótica valley (~25–15 Ma). The ARD caused the kaolinization and impregnation with chrysocolla and copper wad of the bedrock of the Exótica deposit.
(2) The sedimentation of the Fortuna gravels in the Exótica valley starts at ~19 Ma, and intercepts the inflow of Cu-Mn-Si-dominated ARD from Chuquicamata. This was the start of the syn-sedimentary exotic copper mineralization and strong kaolinization of the host gravels.
(3) Tectonic freezing and onset of hyper-aridity (~15 Ma) initiated the oxidation of the enriched chalcocite blanket at Chuquicamata. The resulting Cu-Si-dominated ARD flowed underground into the gravels, resulting in a second

event of chrysocolla mineralization in relatively unaltered gravels. This process lasted at least until 11 Ma.

(4) Finally, between ~6 and 3 Ma, saline groundwater intrusion into the upper part of the Chuquicamata oxidation zone caused the dissolution of Cu-sulfates. The resulting near-neutral, copper- and sulfate-rich solutions precipitated in the upper part of the Chuquicamata supergene profile and further south in the Exótica valley mainly in the northern and central part of the Exótica deposit, as an atacamite/brochantite assemblage over the chrysocolla mineralization.

The ARD at Chuquicamata during the oxidation of the sulfidic ore contained high Fe concentrations from pyrite/chalcopyrite oxidation and biotite weathering; Cu as the dominant dissolved metal cation, and Mn from dissolution of minerals such as rhodochrosite. During oxidation, Fe(III) hydroxides precipitated first due to their low solubility under oxidizing conditions even at very low pH. Jarosite-schwertmannite-goethite precipitated in the 2–4 pH range, retaining most of the iron in the oxidation zone. In this pH range, Mn is mainly present as soluble Mn^{2+} and can precipitate as birnessite at pH ~ 3 and oxic conditions as found in superficial run-off (Dold et al. 2022). The Mn^{2+} and Cu^{2+} cations and the anions SO_4^{2-}, CO_3^{2-}, PO_4^{3-}, $H_3SiO_4^-$, and $H_4SiO_4^\circ$ were mainly leached from the Chuquicamata oxidation zone towards Exótica under acidic conditions. Along the flow path within the Fortuna gravels, the pH and solute activities increased by water–rock interaction and evaporation (Fernández-Mort et al. 2018). The sequence of formation of secondary minerals at Exótica was controlled by the hyperarid climate (Dold et al. 2022). Evaporation and concomitant supersaturation induced mineral precipitation. It is known that high evaporation rates may trigger capillary transport and enrichment of Cu-rich salts on the surface of oxidized ores (Jarrell 1944) or mine wastes (Dold and Fontboté 2001; Dold 2006; Smuda et al. 2014). The geochemistry of this process has been modeled (Bea et al. 2010; Murray et al. 2021). However, the geochemistry of water-polymer interactions and the controls on element activities in a gel-like matrix are little understood.

Material and methods

Samples and field measurements

Gels were sampled in 2009 and 2011 at three sites of gel formation. The site I, located at the extreme south of Exótica, above the pit lake, was sampled during 2009. The sites II and III in the northeastern part of the Exótica pit were sampled in 2011 (Fig. 1 and ESM Fig. 1). Site I was not accessible for resampling in 2011. At this area, the formation of gels was significant and continuous. During exploitation in the southern part of the Exótica deposit, two wells (CHP3 and CHP5) were operating to prevent groundwater inflow into the open pits (Fig. 1). The formation of copper gels as well as the pit lake started when the pumping stopped in 2005 (CODELCO, pers. comm.), and lasted several years. This process is shown in a Google Earth aerial image of 2006 and photographs taken in 2009 and 2011 (Fig. 1). Samples (EX1 and EX2) at site I were collected from a small boat (Fig. 1G and Fig. 1H). At site II, gel samples (2N and 2S) were taken at the water outflow on the pit wall (Figs. 1C, D and ESM Figs. 1A, C, E, G), where the water seeped through the kaolinized and mineralized bedrock. At site III, samples were taken from gels formed on the ground along the outflow of water that had percolated through a chrysocolla and copper pitch mineralized area (samples with the number 7; Figs. 1A, B and ESM 1A, B, D, F). In this area, various drills were performed for blasting operations (ESM Fig. 1A). Only in site III a thin (~ 1 mm thick) green crust was observed underneath the 2–3-cm-thick blue gels that were in direct contact with the ground (Fig. 1B and ESM Fig. 1F). The pH and temperature were measured with a WTW pH meter. All water samples were filtered through 0.2 µm nylon syringe filters. The samples for cation analysis were acidified with suprapure HNO_3. Those for anion analysis were not acidified, only filtered, and stored at 4 °C until analysis. The gels were sampled by filling 250 mL plastic (HDPE) bottles, with the care of minimizing the amount of supernatant water, then tightly closed, and stored at 4 °C.

The potential sources of sulfate in the Calama basin were sampled, including samples of the atacamite/brochantite/gypsum mineralization of Exótica (samples EX3a and EX3b), gypsum from a vein crosscutting the massive chrysocolla mineralization of Exótica (sample EX4), gypsum precipitating during the 2011 sampling campaign on the east wall of the Exótica open pit (sample EX5), and gypsum and anhydrite from the Cordillera de la Sal, ca. 90 km east of Chuquicamata (samples CS1 and CS2, respectively).

Analysis

Microstructural analysis of dry gels was performed using secondary electron (SE) and backscattered electron (BSE) images obtained with a TESCAN Mira LMU Scanning Electron Microscope (SEM) operated at 20 kV acceleration voltage at the University of Lausanne, Switzerland. The microstructure of wet gels was studied using environmental scanning electron microscopy (ESEM) at CSEM SA (Neuchâtel, Switzerland) using a Philips ESEM XL30 FEG at 20 kV with a 2 nm resolution. For the ESEM measurements, the sample was mounted on a Peltier stage and kept with water vapor to perform observations at 100% relative humidity. Mineralogical analysis by X-ray diffraction (XRD) was

performed using a Thermo-Xtra (ARL) instrument (wavelength 1.5406 Å Cu$K\alpha$, continuous scan, THERMO ARL water-cooled silicon detector) at the University of Lausanne, Switzerland. Further XRD analyses of the gel samples were performed after 1 year of storage at 4 °C with a PANalytical Empyrean (Eindhoven, the Netherlands) at the University of Geneva, Switzerland. Infrared spectroscopy (IRS) was used to further investigate the mineralogy of gels and group and compare samples. The IRS analyses (4000–600 cm^{-1} range, co-addition of 64 scans, 4 cm^{-1} resolution) were performed at the University of Lausanne using a Perkin Elmer spectrum 100 FTIR spectrometer with a smart endurance single bounce diamond ATR cell. Prior to IRS, the excess water on gel surface was removed carefully (immersion in liquid nitrogen, wiped off) to minimize water background. In situ qualitative chemical analysis was performed by scanning electron microscopy/energy dispersive X-ray spectrometry (SEM/EDS).

Bulk chemical composition of the dried (100 °C for 24 h) gel samples was determined by XRF analysis using a Philips/PANalytical X-ray fluorescence spectrometer PW 2400 at the University of Lausanne. Major elements were identified and quantified using the program UniQuant, with detection limits set at 10 mg kg^{-1} for all analyses. Water samples were analyzed for Al, As, Ca, Co, Cu, Fe, K, Mg, Mn, Mo, Na, Ni, P, Se, Si, Sr, Ti, and Zn by ICP-OES (iCAP 6300 Duo from Thermo Scientific) at the Faculty of Sciences, University of Geneva, Switzerland. Calibration standard solutions were prepared from mono-elemental solutions (SCP science, Courtaboeuf, France) and the quality of the analyses was checked by analyzing international (NIST SRM 1643e) and laboratory (LPCS-01R-5, lot N°211,025,121–01) standards.

The sulfur and oxygen isotope compositions ($\delta^{34}S$ and $\delta^{18}O$) of dissolved sulfate in water and gel samples and potential sulfur sources (e.g., gypsum and anhydrite) were determined at the stable isotope laboratories of the University of Lausanne. Sulfur isotope analysis was performed by an elemental analyzer (Carlo Erba 1108) coupled to a Thermo Fisher (Bremen, Germany) Delta V Plus isotope ratio mass spectrometer (EA/IRMS system) that was operated in the continuous helium flow mode via a Conflo III split interface (Spangenberg et al. 2010). The oxygen isotope analyses were performed with a Thermo Finnigan high-temperature conversion elemental analyzer (TC/EA) coupled to a Delta Plus XL isotope ratio mass spectrometer (TC/EA/IRMS system). The sulfur and oxygen isotope compositions are reported in the delta (δ) notation as the per mil (‰) deviation of the isotope ratio relative to known standards: $\delta = [(R_{sample} - R_{standard}) / R_{standard}]$, where R is the ratio of the heavy to light isotopes ($^{34}S/^{32}S$, $^{18}O/^{16}O$). For sulfur, the standard is the Vienna Cañon Diablo Troilite (VCDT) and for oxygen the Vienna Standards Mean Ocean Water (VSMOW). The measured $\delta^{34}S$ and $\delta^{18}O$ values were normalized to the VCDT and VSMOW scale using the international reference barium sulfate standards IAEA-SO-5 ($\delta^{34}S = 0.49 \pm 0.11$‰, $\delta^{18}O = 12.13 \pm 0.33$‰), IAEA-SO-6 ($\delta^{34}S = -34.05 \pm 0.08$‰, $\delta^{18}O = -11.35 \pm 0.31$‰), and NBS-127 ($+20.32 \pm 0.36$‰, $\delta^{18}O = 8.59 \pm 0.26$‰). The overall analytical reproducibility of the EA/RMS and TC/EA/IRMS analyses assessed by replicate analyses of barium sulfate laboratory standards ($\delta^{34}S = 12.5$‰, $\delta^{18}O = 12.06$‰) and unknown samples were better than ± 0.2‰ (1 SD). The accuracy of the $\delta^{34}S$ and $\delta^{18}O$ analyses was checked periodically by analyses of the international reference standards. The hydrogen and oxygen isotope compositions ($\delta^{2}H$ and $\delta^{18}O$ in ‰ vs. VSMOW) of gel-associated waters were determined by wavelength-scanned cavity ring-down spectroscopy (WS-CRDS, Picarro L-1120i; Picarro Inc., Santa Clara, CA, USA). The analytical reproducibility was better than 0.3% and 0.1% (1 s) for $\delta^{2}H$ and $\delta^{18}O$ values, respectively.

Evaporation/precipitation experiments were performed to study the salts formed by drying of the gel-associated waters. The geochemical evolution of the gels with time was studied. After 8 months of storage at 4 °C, the gel-water solutions were homogenized, and 1 mL aliquots were filtrated (through 0.2 µm filters) and analyzed for major and trace elements by ICP-OES as described above. The chemistry of these aged waters was compared with that of those analyzed shortly after their collection in the field. Development of crystalline phases in gels with time was investigated by XRD analyses regularly performed on both humid and dried gel samples during 15 months. Two procedures were used to study the formation of minerals in wet gels. The first procedure consisted of XRD analysis on wet gels. The gels with their associated water were covered with cellophane foil to ensure humid conditions and low evaporation during measurements; the XRD analysis was repeated until the gel was completely dry. In the second procedure, a drop of the wet gel was placed in the chamber and the XRD analysis was started immediately. After the analysis, the gel was allowed to dry, and the analysis was repeated 24 h later. The second procedure was replicated eight times during 1 year.

The environmental scanning electron microscope (ESEM) was used to visualize the formation of mineral phases in wet gels. A droplet of the gel was set on the ESEM sample holder (Fig. 2). The ESEM observations started at 100% relative humidity, which slowly decreased. Micrographs were taken at 5.8, 4.9, and 2.5 Torr, corresponding to approximately 95, 80, and 40% relative humidity, respectively.

The saturation indices of the different mineral phases were calculated using the geochemical code PHREEQC (Parkhurst and Appelo 2013). The LLNL database was complemented with data of additional minerals, including libethenite, pseudomalachite, devilline (Majzlan et al. 2015), and posnjakite (Zittlau et al. 2013).

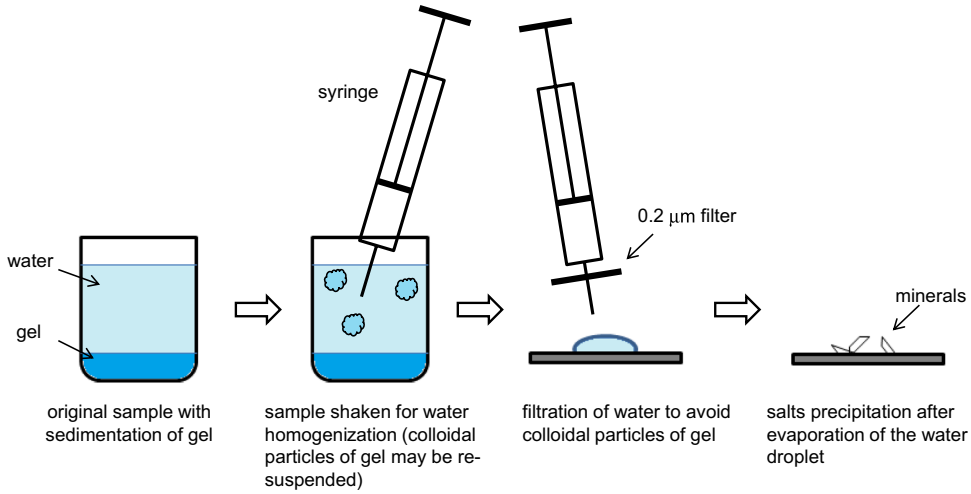

Fig. 2 Experimental setup used to identify the minerals that precipitate after filtration and evaporation of the gel-associated solutions

Results and discussion

Field observations, mineralogy, and geochemistry of the gels

In the field, the color of gels was generally light blue; at two locations, greenish colors were observed. Particularly, in the northern part of the pit (site III), a greenish crust of malachite ($Cu_2CO_3(OH)_2$) was present below light blue gels (Figs. 1A and B). A massive greenish gel occurred on the pit wall in the southern part of the pit (site I; Fig. 1H). This gel is composed of pure atacamite, the Cu hydroxide chloride ($Cu_2(OH)_3Cl$) (Malcherek et al. 2018). Immediately after sampling, gels released water (between 80 and 90% of the initial volume). The pH increased in all gels in the first 8 months and stabilized after 1 year (ESM Fig. 2).

The minerals identified in dried gels by XRD are summarized in Table 1. The dominating Cu-sulfate hydroxides were spangolite ($Cu_6Al(SO_4)(OH)_{12}Cl{\cdot}3H_2O$), posnjakite ($Cu_4(SO_4)(OH)_6{\cdot}H_2O$), schulenbergite ($((Cu,Zn)_7(SO_4)_2(OH)_{10}{\cdot}3H_2O$, together with devilline $CaCu_4(SO_4)_2(OH)_6{\cdot}3H_2O$, serpierite ($Ca(Cu,Zn)_4(SO_4)_2(OH)_6{\cdot}3H_2O$), and trace amounts of brochantite ($Cu_4(SO_4)(OH)_6$), connellite $Cu_{36}(SO_4)(OH)_{62}Cl_8{\cdot}6H_2O$, and montetrisaite $Cu_6(SO_4)(OH)_{10}{\cdot}2H_2O$. Other Cu phases present in trace amounts include atacamite ($Cu_2(OH)_3Cl$, Malcherek et al. 2018) and malachite ($Cu_2(CO_3)$

Table 1 Overview of minerals identified in Exótica gels

Name	Abbreviation	Chemical formula	Gel group 1				Gel group 2		Gel group 3
			7B	7C1	7C2	EX1	2N	2S	EX2
Atacamite	ata	$Cu_2(OH)_3Cl$ *							
Blödite	bl	$Na_2Mg(SO_4)_2{\cdot}4H_2O$							
Brochantite	br	$Cu_4(SO_4)(OH)_6$							
Connellite	con	$Cu_{36}(SO_4)(OH)_{62}Cl_8{\cdot}6H_2O$							
Devilline	dv	$CaCu_4(SO_4)_2(OH)_6{\cdot}3H_2O$							
Gyspum	gy	$Ca(SO_4){\cdot}2H_2O$							
Halite	hl	NaCl							
Malachite	mal	$Cu_2(CO_3)(OH)_2$							
Montetrisaite	mts	$Cu_6(SO_4)(OH)_{10}{\cdot}2H_2O$							
Posnjakite	psj	$Cu_4(SO_4)(OH)_6{\cdot}H_2O$							
Schulenbergite	sch	$(Cu,Zn)_7(SO_4)_2(OH)_{10}{\cdot}3H_2O$							
Serpierite	sp	$Ca(Cu,Zn)_4(SO_4)_2(OH)_6{\cdot}3H_2O$							
Spangolite	spg	$Cu_6Al(SO_4)(OH)_{12}Cl{\cdot}3H_2O$							
Thénardite	th	Na_2SO_4							

*After Malcherek et al. (2018)

Table 2 Elemental composition of the dried gels from Exótica

Sample	Na_2O wt.%	MgO wt.%	Al_2O_3 wt.%	SiO_2 wt.%	MnO wt.%	Fe_2O_3 wt.%	P_2O_5 wt.%	K_2O wt.%	CaO wt.%	TiO_2 wt.%	SO_3 wt.%	Cl wt.%	Cu wt.%	Zn wt.%
2 N	bdl	0.34	5.27	1.69	0.07	0.50	bdl	0.32	2.36	0.02	15.7	1.28	57.5	0.06
2S	bdl	0.76	1.43	6.23	0.12	1.05	0.01	0.80	5.36	0.07	19.8	1.55	49.4	0.52
7C1	5.20	2.33	3.06	3.45	0.13	0.77	0.01	0.88	7.43	0.05	23.4	3.32	39.1	0.39
7C2	bdl	1.01	3.02	2.28	0.12	0.65	0.02	0.78	6.89	0.04	21.7	3.38	47.1	0.43
EX3b	bdl	bdl	bdl	0.64	0.01	0.02	0.04	bdl	0.22	bdl	12.6	3.89	65.9	0.03
EX1	bdl	0.35	5.22	1.31	0.32	0.10	0.95	0.10	1.11	0.01	13.4	3.54	58.5	0.23
EX2	bdl	bdl	2.66	2.81	0.07	0.36	0.26	0.13	0.51	0.02	2.48	13.4	61.6	0.11
Malachite crust	bdl	1.45	6.20	20.8	0.32	3.06	0.10	0.94	1.16	0.22	1.27	0.04	50.9	0.48

bdl, below detection limit

$(OH)_2$). The non-Cu minerals were predominantly gypsum ($CaSO_4{\cdot}2H_2O$), blödite ($Na_2Mg(SO_4)_2{\cdot}4H_2O$), and traces of thénardite (Na_2SO_4) and halite (NaCl).

In all gels, copper is the main component (39–62 wt%), followed by SO_3 (2.5–23.4 wt%), Cl (1.3–13.4 wt%), CaO (0.5–7.4 wt%), Al_2O_3 (1.4 and 5.3 wt%), and SiO_2 (1.3 and 6.2 wt%) (Table 2). The dominant elements in gel EX2 are Cu and Cl (61.6 and 13.4 wt%, respectively), whereas Cu and S are the most abundant elements in the other gels. Sample 2S has the highest SiO_2 content (6.2 wt%), which is more than in the other gels (Table 2). However, these low SiO_2 contents of the gels contrast with those of the chrysocolla samples from the Exótica deposit (26–43 wt% SiO_2).

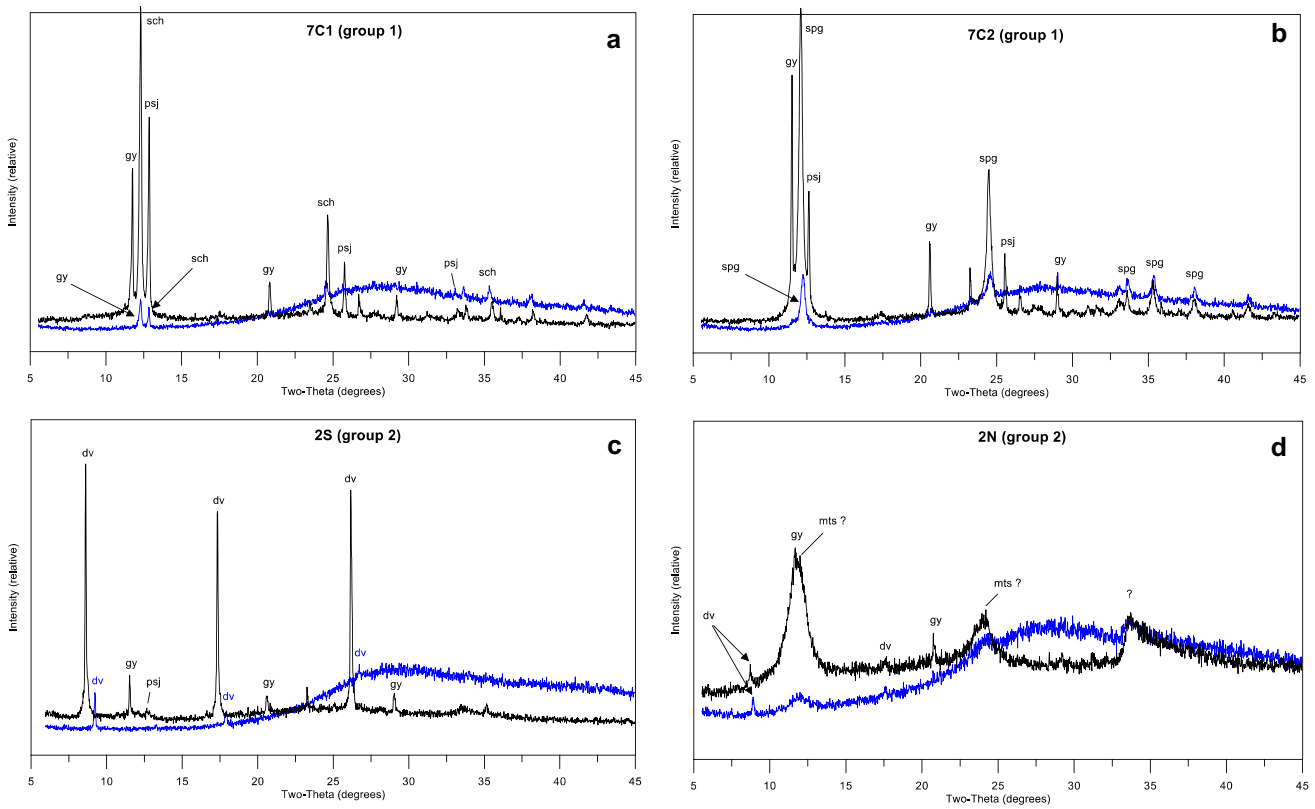

Fig. 3 Comparison of XRD spectra of humid (blue) and dried (black) gels. **a**, **b** Samples 7C1 and 7C2 from gel group 1 (site III). **c**, **d** Samples 2S and 2 N from gel group 2 (site II). In all XRD spectra, the peaks obtained under humid conditions are slightly displaced to the right compared with the peaks obtained for dried gels. Note in **d** the characteristic broad peaks (around 12, 24, and 33 degrees) observed only in this gel (sample 2 N). Abbreviations: dv, devilline; gy, gypsum; mts, montetrisaite; sch, schulenbergite; spg, spangolite; psj, posnjakite

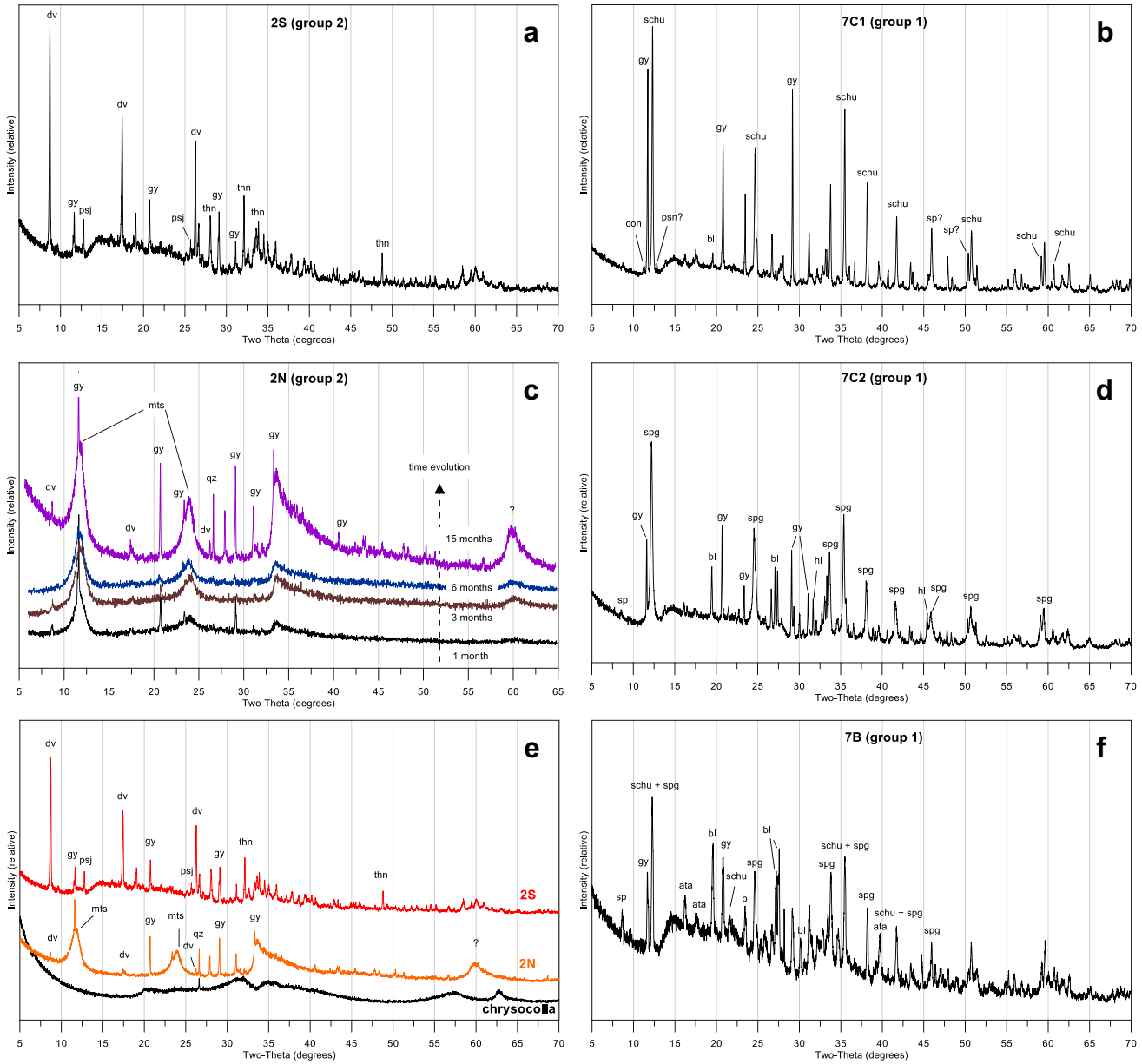

Fig. 4 XRD spectra of dried gels with samples from site II on the left colon (**a**, **c**, **e**) and samples from site III on the right (**b**, **d**, **f**). **a** Sample 2S from gel group 2. **b**, **d**, **f** Samples 7C1, 7C2, and 7B from gel group 1. **c** Various XRD spectra of sample 2 N from gel group 2 taken over a year, highlighting the development of broad peaks with time (e.g., broad peak at 60 degrees), possibly indicating the development of a poorly crystalline phase. **e** Comparison of XRD spectra of chrysocolla from Exótica mineralization (sample MC24) and gel samples 2 N and 2S. Of note are the broad peaks of chrysocolla, which are not aligned with the broad peaks observed in gel 2 N (e.g., peak at about 63 degrees in chrysocolla and at about 60 degrees in gel 2 N). Abbreviations: ata, atacamite; bl, bloedite; dv, devilline; gy, gypsum; mts, montetrisaite; psj, posnjakite; sch, schulenbergite; spg, spangolite; thn, thenardite

The mineralogical and chemical composition of the gels (Tables 1 and 2, Figs. 3 and 4), combined with the pH (ESM Fig. 2), and elemental composition of the associated waters (Table 3) allowed to distinguish three different gel groups.

Gel group 1 is defined by the samples 7B, 7C1, and 7C2, which have schulenbergite as the dominant mineral when the pH of the associated waters is the lowest (pH ~ 6.0) or spangolite as the most abundant mineral when the pH is slightly higher (~ 6.4) (Tables 1, 2, and 3, Figs. 3a, b and 4b, d, f). Other Cu phases present in trace amounts include brochantite, connellite, serpierite, atacamite, and malachite. The Cu-free minerals are blödite, gypsum, and halite. In sample 7C2, the XRD peaks of gypsum appeared only after complete drying of the gel,

Table 3 Major anions and cations and trace elements composition of the gel supernatant solutions

Sample	Main mineral in gel	Field measurements			F	Cl	Br	Acetate	NO_3	PO_4	SO_4	Li	Na	NH_4	Mg	Al	Si	K	Ca	Mn
		Eh [mV]	T [°C]	pH	mg/L	mg/L	mg/L	mg/L	mg/L	mg/L	mg/L	mg/L	mg/L	mg/L	mg/L	mg/L	mg/L	mg/L	mg/L	mg/L
W5	Gypsum	420	14.0	7.41	bdl	8224	bdl	bdl	10,870	43.2	5227	1.38	10,380	44.8	359	1.37	2.35	74.9	985	10.7
EX1	Spangolite	-	21.3	5.79	14.0	3302	1.55	-	4319	0.11	13,314	3.54	6125	0.90	1156	3.76	22.0	106	484	344
EX2	Atacamite	-	18.4	5.67	20.8	16,777	7.78	-	14,174	0.73	7047	4.90	13,325	1.91	1907	9.37	20.3	220	1246	411
WG2S	Devilline	535	6.50	6.82	bdl	517	bdl	bdl	713	bdl	4314	0.54	1649	37.3	212	3.32	14.1	134	532	8.17
WG7	Schulenbergite & spangolite	541	22.5	6.13	bdl	1320	bdl	176	2211	bdl	5578	0.74	2756	795	518	1.42	1.80	151	476	5.38
WG7B	Schulenbergite & spangolite	553	21.8	5.89	bdl	1079	bdl	420	1719	bdl	5381	0.84	2163	1720	392	3.91	6.83	141	304	13.3
Sample	Main mineral in related gel	Sc	Ti	V	Cr	Fe	Co	Ni	Cu	Zn	Ga	Sr	Zr	Mo	Ag	Cd	Sb	Cs	Pb	Bi
		µg/L	µg/L	µg/L	µg/L	µg/L	µg/L	µg/L	µg/L	µg/L	µg/L	µg/L	µg/L	µg/L	µg/L	µg/L	µg/L	µg/L	µg/L	µg/L
W5	Gypsum	bdl	0.50	bdl	23.6	619	372	bdl	236	854	10.9	19,600	3188	595	1.60	bdl	bdl	1.80	bdl	bdl
EX1	Spangolite	-	-	2.42	bdl	bdl	4904	1123	184,100	38,590	4.46	8555	-	18.6	bdl	266	bdl	2.18	bdl	bdl
EX2	Atacamite	-	-	5.24	bdl	bdl	5317	1347	239,200	61,600	8.19	20,900	-	bdl	bdl	443	bdl	7.47	56.8	bdl
WG2S	Devilline	bdl	bdl	bdl	5.74	125	153	bdl	134,119	4888	14.3	7162	7375	206	1.83	bdl	bdl	1.32	1.81	bdl
WG7	Schulenbergite & spangolite	bdl	bdl	bdl	24.6	98.8	61.8	bdl	14,832	6746	10.1	9499	2796	127	2.56	9.11	bdl	10.7	3.54	bdl
WG7B	Schulenbergite & spangolite	85.7	bdl	bdl	23.9	101	208	bdl	69,318	19,395	21.7	11,927	6108	441	31.2	156	383	19.4	30.5	43.0

bdl, below detection limit; -, not analyzed

whereas in sample 7C1, gypsum was present in the wet gel (Figs. 3a and b). Additionally, textural differences observed by ESEM characterize the gels 7B and 7C1. The matrix consists of tiny needles and elongated crystals (Figs. ESM 6c, d). In sample 7C1, the most abundant mineral has a ditrigonal pyramidal morphology (ESM Figs. 6a, b, f). This mineral is schulenbergite (Ohnishi et al. 2007), one of the two most common layered Cu-sulfates in this gel together with spangolite (Fennell et al. 2011). Another common mineral in gel 7C1 is connellite, this mineral was not observed in the other gels, and is characterized by radiating acicular crystals (ESM Figs. 6c, d). In the sampling site of group I gels, a thin green crust (~ 1 mm) of malachite was present below the bluish copper gels of this group (Fig. 1B). A similar observation was reported by Majzlan (2020) in an audit of the ancient mining town of Ľubietová (Slovakia), where green malachite crystallize from masses of blue gels. The formation of a malachite crust in contact with a slightly acidic solution (pH < 6.5) is in line with the thermodynamic stability field of this mineral (Plumhoff et al. 2020). The underlying substrate at the site of group I gels had most probably some carbonate buffer capacity, which increased the pH, favoring malachite precipitation in direct contact with the substrate (Melchiorre and Enders 2003). This process is further supported by FTIR data, where the characteristic absorption bands of CO_3^{2-} (1083–1098, 743, 816, and 833 cm^{-1}) indicate the presence of carbonate phases in samples 7C1 and 7C2 (ESM Figs. 3 and 4). The FTIR spectra also suggest that the carbonate might be associated with malachite, and most probably not georgeite ($Cu_2CO_3(OH)_2$. Georgeite is a gel-like copper carbonate hydroxide meta-stable with respect to malachite; it has been proposed as a precursor mineral to malachite in alkaline conditions (Pollard et al. 1991; Lytle et al. 2019). The absence of georgeite is further supported by the slightly acidic pH conditions at site III. The source of copper for the group 1 gels is the chrysocolla from the copper pitch mineralization occurring in the strongly altered gravels. The gel-associated solutions (i.e., gel source solutions) had a pH of 5.9–6.1 (Table 3). After 1 year maturation, the pH evolved to 6.0–6.5 (Fig. ESM 2).

The gels associated to the water outflow at the southern part of the open pit (sample EX1) were formed from groundwaters flowing through the gravels. Therefore, this gel was included in group 1. The only mineral identified in this gel was spangolite. The gel-associated solution had relatively low pH (5.8–6.1), SO_4/Cl weight ratios between 3.08 and 4.99, and SO_4/NO_3 ratios between 2.52 and 3.13.

Gel group 2 is formed by the gel samples 2 N and 2S, coming from site II (Figs. 1C and D). The dominating Cu-sulfate hydroxide in this group is devilline (Table 1, Figs. 3c, d, 4a, c, e, and Fig. ESM 5). The presence of montetrisaite, a recently discovered mineral structurally related to posnjakite and spangolite (Orlandi and Bonaccorsi 2009), in gel 2 N was confirmed by XRD pattern. The broad XRD peaks in this gel, persistent in all the analyses performed during 1 year, were attributed to the presence of at least one poorly crystalline phase (Figs. 3d and 4c, e). None of the other gels showed these broad peaks. Other Cu phases present in trace amounts were spangolite, posnjakite, and malachite. The non-Cu minerals were predominantly gypsum and traces of thénardite. The most abundant Cu-sulfate is devilline, showing a characteristic leaflet texture (Figs. ESM 5a, b, c). The matrix of the group 2 gels had a "sponge-like" structure composed mainly of Cu, O, and S with traces of Si and Al, suggesting that silica was involved in the matrix of these gels (Figs. ESM 5d, e, ESM 7a, b). The pH of the source solutions of group 2 gels had a pH of 6.8, SO_4/Cl ratio of 8.34, SO_4/NO_3 ratio of 6.05, and 532 mg/L of Ca (Table 3). After 1 year maturation, the pH in samples 2 N and 2S were 7.2 and 7.7, respectively (Fig. ESM 2). In site II, the groundwaters flowing through the kaolinized bedrock characterized by propylitic alteration contain most probably calcite and gypsum as a source for Ca^{2+}, CO_3^{2-}, and SO_4^{2-} ions, maintaining pH in a near-neutral range.

Gel group 3 contains only atacamite and is represented by sample EX2 from the southern part of the open pit (site I, Figs. 1H). The water associated with this gel had a pH of 5.7, 16.8 g/L Cl, 14.2 g/L NO_3, 7.0 g/L SO_4, and 239 mg/L Cu (Table 3). The composition of this solution is seen as an expression of the lower saline aquifer of the Calama basin (Fig. 1J). The water outflowing at the eastern part of the pit (sample W5, Fig. 1K) had SO_4/Cl and SO_4/NO_3 ratios similar to those of the solutions associated with gel EX2 (0.48 vs. 0.42 and 0.48 vs. 0.50, respectively), but relatively low concentration of copper (0.24 mg/L). At that site precipitated massive gypsum but no copper minerals due to the low dissolved copper. However, geochemical modeling suggests that the water W5 is supersaturated with respect to atacamite (SI = 1.45). Therefore, sample W5 was included in group 3.

Drying and maturation triggered the precipitation of the different copper sulfate hydroxide phases in the gels. In the three gel groups, some of the minerals found in trace amounts may have formed during the drying of the gel. For example, malachite was not observed when studying wet gels but appeared as traces in dried gels 7B and 2S (Table 1, Fig. 5a). Additionally, under humid conditions, the high background due to water in gels only allowed the FTIR observation of the major, well-crystallized phases. Therefore, we postulate that copper is mainly present in a $CuSO_4$ polymer matrix forming the gel structure, with some minor nanomineral phases already present in the wet gels.

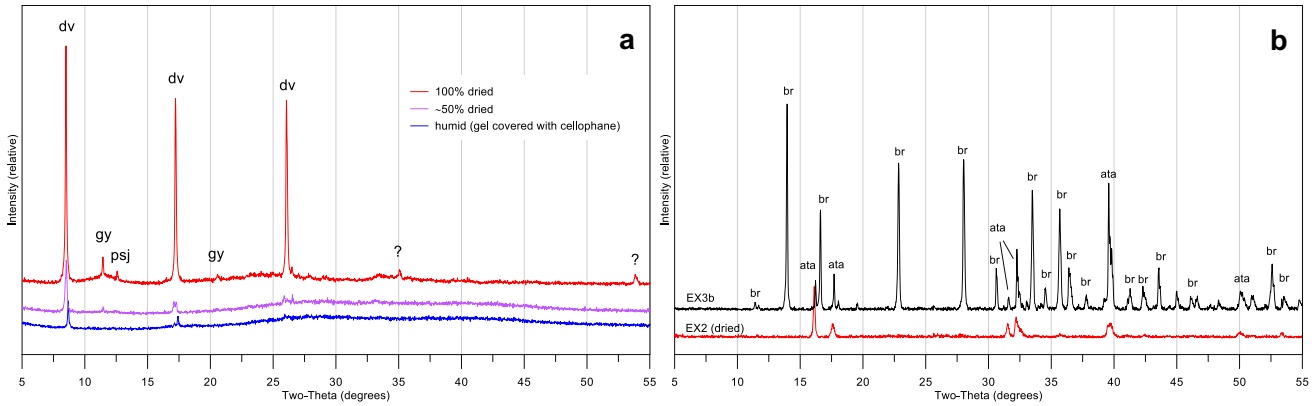

Fig. 5 **a** XRD spectra from a drying gel sample (sample 2S, gel group 2). The first analysis was performed with the sample covered with a thin plastic film (cellophane) to determine if well-crystallized minerals were identifiable under high humidity conditions. The plastic film was then removed, and the analyses were repeated until complete dryness of the gel (red line). **b** XRD spectra of the dried gel sample EX2 (red line) containing only atacamite and the sample EX3b with brochantite and atacamite. Abbreviations: ata, atacamite; br, brochantite; dv, devilline; gy, gypsum; psj, posnjakite

Changes in the hydrochemistry of the supernatant solutions during gel maturation

The differences in the hydrochemistry of gel 7B from group 1 (water samples WG7B and WG7B8; Fig. 1A) and gel 2S from group 2 (water samples WG2S and WG2S8; Fig. 1C) shortly after sampling and after 8 months of storage at 4 °C can be seen in Table 4. The initial composition of the two solutions was different, which is in line with the mineralogical difference of the gels (Table 1). In gel 7B, the water remained slightly acidic (pH 5.9 to 6.0; ESM Fig. 2), and in gel 2S, the water pH slightly increased from 6.8 to 7.5. At sampling, the gel water in 2S had higher concentrations in Al, Si, Cu, and Mo compared to 7B, and was lower in Na, K, Mg, Mn, Sr, P, and Zn; both waters had similar concentrations in Ca. The differences in the chemistry of the gel waters (WG7B, WG2S), which was one criterion used for grouping gels, are the effect of different mixing ratios and solute contributions from groundwaters flowing through rocks with advanced argillic (kaolinitic) and propylitic alteration and waters leaching the Chuquicamata oxidation zone.

After 8 months of storage, the pH increased from 6.8 to 7.8 in WG2S, but remained constant between 5.9 and 6.1 in WG7B (Table 4). The concentration of major cations Na, Mg, K, and Ca remained mainly unchanged in both gel waters (Table 4). In contrast Cu, Co, and Zn concentrations decreased strongly, particularly in the water sample of gel 2S. For copper, this might be explained by an increase in the saturation concentration (saturation index, SI = 1) to supersaturation (SI between 1.14 and 3.94) with respect to antlerite, brochantite, and atacamite (Table 5). These high SI values suggest precipitation of secondary copper sulfate hydroxides during gel-water maturation. The decrease in concentrations of Co and Zn in WG2S may be due to sorption of metal ions on gel at circumneutral pH. In contrast, in the slightly acidic water of gel 7B, the small increase in Co and Zn suggests that these metals may have been liberated by dissolution, desorption, and/or equilibrium processes during the storage period (Table 4).

Finally, the saturation indices calculated with PHREEQC from the analyses of the different gel-associated waters and for several solid phases (Table 5) provide further insight into the relationship between the hydrochemistry and mineralogy of gels. Chalcanthite ($CuSO_4{\cdot}5H_2O$), halite, and chrysocolla ($((Cu_{2-x}Al_x)H_{2-x}Si_2O_5(OH)_4{\cdot}nH_2O$) were undersaturated in all samples (Table 5), thus explaining why these minerals were not detected in these gels. The stable Cu-sulfate hydroxides brochantite and antlerite ($Cu_3(SO_4)(OH)_4$) and the Cu chloride hydroxide atacamite were supersaturated in most waters, except for WG2S, which reached supersaturation in respect of these minerals after 8 months of maturation (Table 5). Both minerals, brochantite and antlerite, were not detect by XRD in the dried gels 7B and 2S (Table 1). Devilline was identified in the group 2 gels, and posnjakite in gels of groups 1 and 2 (Table 1), despite being strongly undersaturated in all waters. The water sample W5 associated with the precipitation of gypsum was only supersaturated in respect to atacamite (Fig. 1, Table 5). These contrasting results point to limitations in the geochemical modeling of gel-type matrices, which may be complex multicomponent systems as described above for the Exótica gels.

Mineral precipitation sequence during evaporation of the gel supernatant solution

The comparison of XRD spectra of humid and dried gels of groups 1 and 2 (Fig. 3) and the XRD analysis of a gel repeated over a year (Fig. 4c) provided some insight on the

Table 4 Hydrochemistry of the gel supernatant solutions at sampling and after 8 months storage at 4 °C

Sample	Description	pH	Al	Ca	Co	Cu	K	Mg	Mn	Mo	Na	P	Si	Sr	Ti	Zn
			mg/L	mg/L	mg/L	mg/L	mg/L	mg/L	mg/L	mg/L	mg/L	mg/L	mg/L	mg/L	mg/L	mg/L
WG2S	Gel-water directly after sampling	6.82	1.51	582	0.18	138	142	244	8.32	0.24	1753	4.38	14.1	8.51	0.04	5.20
WG2S8	Gel-water after 8 months storage	7.75	bdl	492	0.01	0.44	144	274	3.45	0.35	1864	4.22	2.66	8.21	0.03	0.67
WG7B	Gel-water directly after sampling	5.89	0.07	575	0.20	63.6	199	676	12.5	0.10	3002	8.87	6.83	11.9	0.04	17.0
WG7B8	Gel-water after 8 months storage	6.13	0.56	490	0.32	54.3	215	752	19.2	0.06	3145	9.20	9.64	12.6	0.04	38.1

bdl, below detection limit

precipitation of mineral salts in evaporating and maturing gel. The mineral phases and their precipitation sequence during evaporation of the filtered supernatant solution from gels (Fig. 2) were further investigated by SEM and SEM/EDS analyses. It was confirmed that gypsum crystals were the first to grow, some with typical twins and up to 0.5 mm in length (Fig. 6a). The gypsum crystals were then covered by sodium sulfate crystals with a lenticular habit (gels 7C1, 2 N, and 2S; Fig. 6b, c, d). These sodium sulfates contained magnesium and were up to 20 µm in length and 5 µm in width. Crystals with the same chemistry (i.e., Na, S, and O) were present in all samples, but not always (i.e., gel 7C2) with lenticular habit. Cubic crystals of halite were visible in samples 2 N and 2S (Fig. 6b and c). Finally, unidentified nano-needles (< 500 nm) were covering some of the above-mentioned minerals, particularly in samples 7C1 and 2 N (Fig. 6d).

The crystallization sequence of mineral phases precipitating during evaporation of the gel supernatant waters follows the increasing solubility order: gypsum → Na(Mg) sulfate (e.g., blödite) → halite. This sequence of mineral-salts precipitation is in line with the field observations. Gypsum — the major non-Cu mineral in the gels — often occurs as white bands intercalated within banded ores of greenish Cu-sulfate hydroxides and chlorides (Fig. 7a). In the drying gel-associated solution, most of the dissolved copper was first incorporated into minerals (mainly copper sulfate hydroxides) and possibly in the gel matrix. This is in line with the lower solubility of Cu-sulfate hydroxides (i.e., antlerite and brochantite) compared to gypsum (Zittlau et al. 2013). Therefore, we can assume that the solutions that lead to the formation of the exotic ores precipitated first most of the dissolved Cu as copper sulfate hydroxides (brochantite, antlerite) and copper sulfate hydroxide hydrates (e.g., chalcanthite and devilline). The excess of sulfate precipitated later as gypsum when dissolved calcium was available. The high solubility of the other salts (e.g., sodium sulfate and halite) explains why they are rarely found in oxide ores.

Sulfur isotope composition and source of sulfur

The sulfur isotope compositions ($\delta^{34}S$ value) of the sulfur-containing phases in bedrock (sulfides and sulfates), gel, and water samples were used to investigate the sulfur source for the Exótica deposit. The principal sources of sulfate sulfur in the Chuquicamata-Calama region are the oxidized primary sulfides of the Chuquicamata ore (Smuda et al. 2014) and sulfate minerals derived from weathering (Carmona et al. 2000; Rech et al. 2003). The $\delta^{34}S$ values of the primary sulfide mineralization at Chuquicamata range from − 5.4 to 2.6‰ and those of the primary sulfates (e.g., anhydrite-gypsum) from 2.1 to 16.4‰ (Smuda et al. 2014). The primary gypsum and anhydrite samples from the sedimentary formation of the Cordillera de la

Table 5 Saturation indices (SI) of selected copper sulfate hydroxides and chlorides for the gel supernatant solutions

Sample	pH	pe	Devilline	Posnjakite	Chalcanthite	Antlerite	Brochantite	Atacamite	Tenorite	Chrysocolla	Gypsum	Halite
W5	7.41	7.1	−46.9	−86.5	−6.46	−1.66	−0.30	1.45	0.42	−2.59	−0.32	−2.94
EX1	5.79	8.5	−32.8	−82.4	−2.64	2.35	3.82	4.35	0.52	−1.48	−0.10	−3.57
EX2	5.69	8.5	−32.8	−83.1	−3.05	1.78	3.14	5.55	0.42	−1.63	−0.15	−2.53
WG7B	5.89	9.3	−34.9	−83.7	−3.24	1.31	2.56	2.38	0.30	−2.06	−0.34	−4.45
WG7B8	6.13	9.3	−35.6	−83.1	−3.53	1.61	3.16	3.06	0.60	−1.77	−0.22	−4.29
WG2S	6.82	9.0	−49.7	−88.4	−7.58	−3.32	−2.20	−6.35	0.16	−5.03	−4.76	−4.84
WG2S8	7.75	9.0	−44.4	−82.3	−5.69	1.14	3.94	3.18	1.58	−1.35	−0.07	−4.78

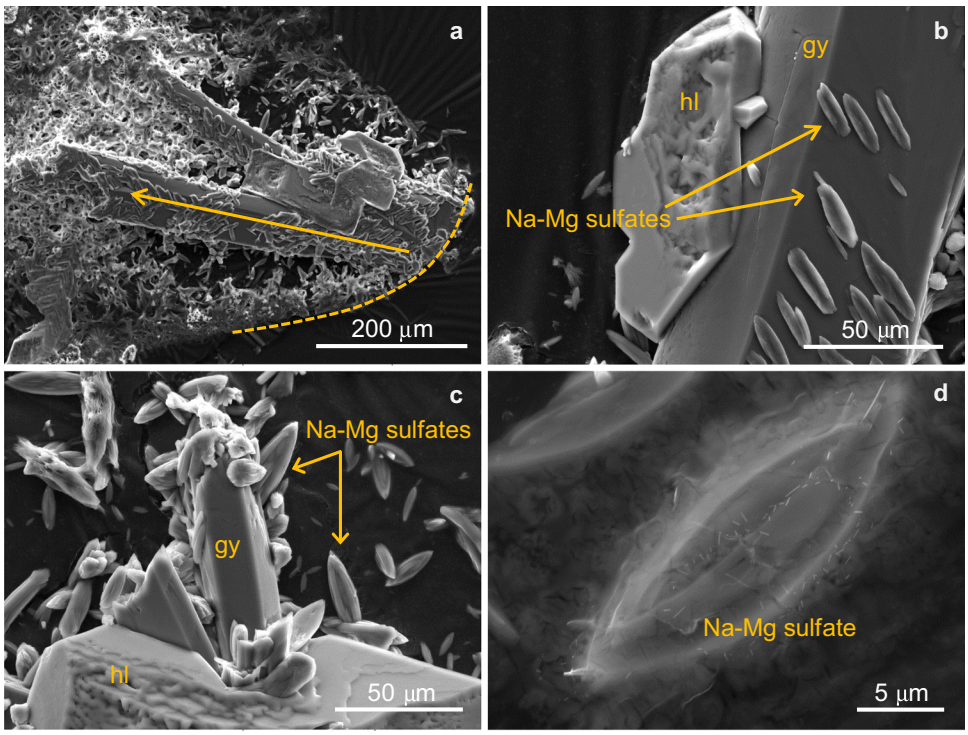

Fig. 6 Crystallization sequence deducted from SEM micrographs. **a** Gypsum growing first from the water droplet edge (dashed line) towards the interior of the droplet (gel 2 N). **b** Gypsum, Na-(Mg)-sulfate and halite (gel sample 2 N). **c** Halite (hl) covering gypsum and Na-(Mg)-sulfate (gel sample 2S). **d** Typical lenticular morphology of Na-(Mg)-sulfate covered by nano "needle like" minerals (gel sample 7C1). Abbreviations: gy, gypsum; hl, halite

Sal, located 90 km southeast of Chuquicamata, have both a $\delta^{34}S$ value of 3.1‰ (Table 6, Fig. 8). This value is close to the $\delta^{34}S$ value of 3.7‰ obtained by Rech et al. (2003) for gypsum from the same geological formation. Similar $\delta^{34}S_{sulfate}$ values were also measured in groundwaters below the Talabre tailings impoundment (Smuda et al. 2014). Such $\delta^{34}S_{sulfate}$ values are within the range typical for local streams, lakes, and salt lakes in the Atacama Desert, and are assumed to be representative of weathering of primary sulfides (3 to 7‰, Carmona et al. 2000; Rech et al. 2003). The gypsum and dissolved sulfate in the groundwater outflow at the east wall of the Exótica pit have $\delta^{34}S$ values of 1.3 and 1.6‰, respectively (samples EX5 and W5, Fig. 8). In the Exótica ore, the sulfate minerals in a single hand specimen of banded ore show a range of 2.6‰ in the $\delta^{34}S$ values (Fig. 7a). A value of −2.1‰ was measured in the greenish atacamite/brochantite layer (sample EX3b) and a value of 0.5‰ in the open-space filling gypsum (sample EX3b) (Table 6, Fig. 7a–c). Additionally, the gypsum crosscutting the chrysocolla mineralization has a $\delta^{34}S$ value of −0.4‰ (sample EX4, Table 6). The $\delta^{34}S$ value for atacamite/brochantite suggests that sulfur originated from oxidation of primary sulfides from Chuquicamata (Smuda et al. 2014). The relatively higher $\delta^{34}S$ value of the gypsum suggests mixing of a ^{34}S-depleted fluid (i.e., ~ −2‰) with an incoming isotopically heavier dissolved sulfate-sulfur, most probably from leaching the gypsum-anhydrite deposit of local sedimentary formation (e.g., Cordillera de la Sal). This incoming Ca-SO_4-rich and neutral groundwater would be similar to the water outflowing at the east wall of the Exótica pit, which carried dissolved sulfate with 1.6‰ $\delta^{34}S$ (sample W5, Table 6). The sulfur isotope composition of gels was studied in the dissolved sulfate in the gel-associated waters and in dry gels. Both the $\delta^{34}S$ values of

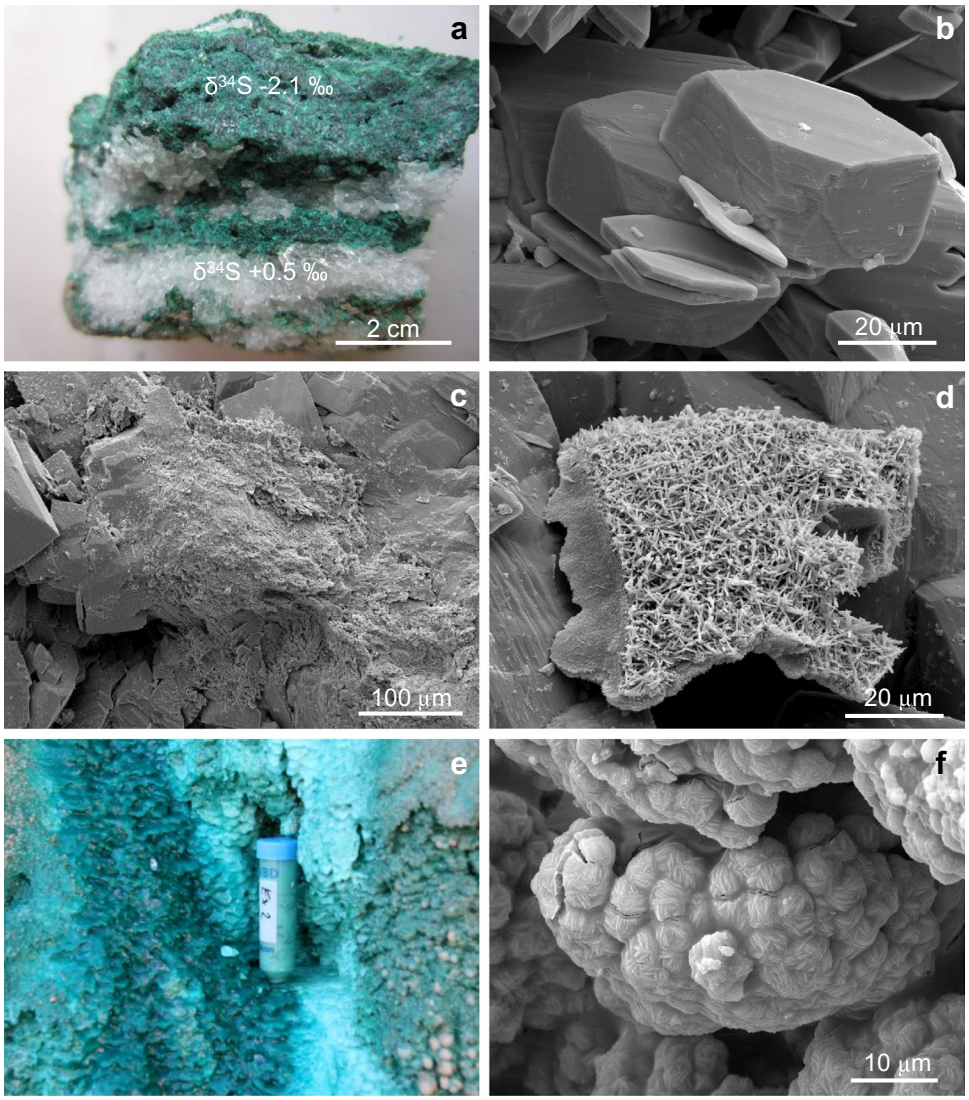

Fig. 7 **a** Atacamite/brochantite mineralized sample from Exótica associated with gypsum (white bands) with $\delta^{34}S$ values of + 0.5‰ (sample EX3a) and Cu-sulfates (green) with $\delta^{34}S$ values of − 2.1‰ (sample EX3b). **b**–**d** SEM micrographs of green bands from **a**. **b** Characteristic idiomorphic crystal of brochantite. **c** Atacamite covering brochantite. **d** Nano-needles of Si and Al (major elements detected by EDS). **e** Pure atacamite gel above the Exótica open pit lake (sample EX2, site I). **f** SEM micrograph of dried gel sample EX2 showing the atacamite morphology

the dissolved sulfate (− 1.0 and − 0.6‰) and of the bulk dried gels (− 1.3 and − 1.0‰; Table 6) are negative. These slightly negative values suggest that the sulfur source in the Exótica gels is primarily the oxidation of sulfides rather the sulfate of sedimentary origin. Therefore, the sulfate-sulfur in the gels was derived chiefly from groundwaters interacting with the exotic mineralization known south of the Exótica pit, which was then exploited after sampling.

Sulfate/chloride ratio, copper concentration, and effects of salinity on mineralization

The sulfate/chloride ratio of the waters controlled the relative abundance of precipitating copper sulfates (e.g., brochantite, connellite, and devilline) and copper chloride (atacamite). In saline or saline-influenced water samples, SO_4/Cl is ≤ 1 and in non-saline freshwater samples, SO_4/Cl is > 1. The SO_4/Cl ratios of the solutions associated with gels containing copper sulfates hydroxides (gel groups 1 and 2) were between 3.1 and 8.3. In contrast, the solution in gels dominated by atacamite (i.e., gel EX2, group 3) had SO_4/Cl ratio of 0.42. This low SO_4/Cl ratio is similar to the ratio measured in waters of the lower saline aquifer of the Calama basin (i.e., sample W5, $SO_4/Cl = 0.48$). In the brochantite-atacamite-gypsum mineralization, well-crystallized idiomorphic brochantite is covered with atacamite (sample EX3b, Figs. 7a, b, c). This textural relation suggests that the primary supergene copper sulfate precipitated from meteoric water with relatively high SO_4/Cl ratio and was intergrown and overgrown by copper chloride, which started to precipitate when SO_4/Cl was lowered by evaporation, brochantite precipitation, and incursion of saline groundwater. The intruding saline groundwater was most likely linked to the lower saline groundwater level in the Calama basin (Dirección General de Aguas 2003; Jordan et al. 2015), which was also found below the Talabre tailings impoundment (Smuda

Table 6 Stable isotope composition of waters (δ^2H, $\delta^{18}O$) and sulfates ($\delta^{34}S$, $\delta^{18}O$)

Sample	Details of sample	δ^2H (‰ VSMOW)	$\delta^{18}O$ (‰ VSMOW)	$\delta^{34}S$ (‰ VCDT)	$\delta^{18}O$ (‰ VSMOW)
W5	Water associated with gypsum precipitation (no Cu-gel), Exótica	−60.4	−6.34	1.60	7.10
WG2S	Water from gel (main mineral in gel = devilline), Exótica	−72.7	−9.24	−0.60	3.45
WG7	Water from gel (main mineral in gel = schulenbergite & spangolite), Exótica	−63.0	−6.92	-	-
WG7B	Water from gel (main mineral in gel = schulenbergite & spangolite), Exótica	−63.3	−6.96	−1.10	4.51
CS1	Gypsum, Cordillera de la Sal			3.12	8.43
CS2	Anhydrite, Cordillera de la Sal			3.10	10.40
EX4	Gypsum occurring within chrysocolla banded ores, Exótica			−0.41	3.55
EX3a	Gypsum occurring within atacamite/brochantite banded ores (sample from Codelco staff), Exótica			0.50	9.70
EX3b	Atacamite/brochantite banded ores (sample from Codelco staff), Exótica			−2.10	-
EX1	Dried gel EX1, Exótica			−1.30	9.90
EX2	Dried gel EX2, Exótica			−1.00	4.60
EX5	Gypsum precipitation (no Cu-gel), Exótica			1.30	10.80

-, not analyzed

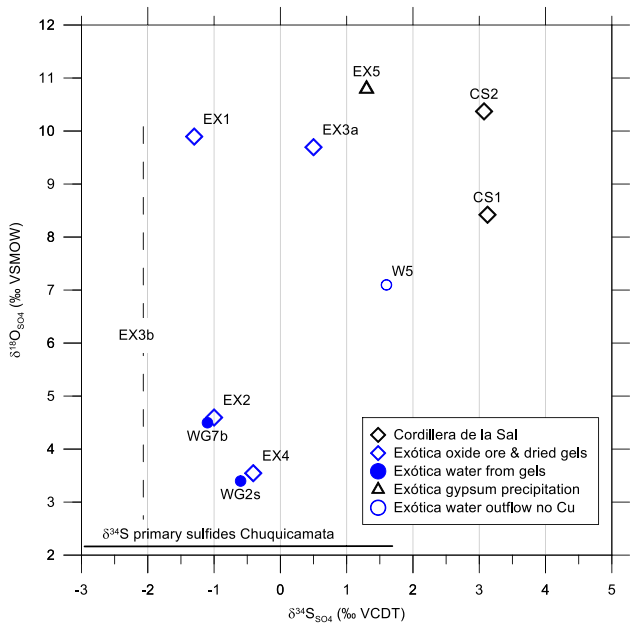

Fig. 8 Oxygen vs. sulfur isotope composition ($\delta^{34}S$, $\delta^{18}O$) of dissolved sulfate in water-associated gels of groups 1 and 2 (water from gel samples 7B and 2S, respectively) and sulfates from the Exótica (Mina Sur) deposit. Sample EX3a is gypsum intercalated between atacamite/brochantite veins (white bands in Fig. 7a). Sample Ex3b is brochantite from the same hand specimen (green bands in Fig. 7a). Sample EX4 is a pure gypsum crystal (specimen ~ 0.5 cm high) within massive chrysocolla. Samples EX1 and EX2 are dried gels from groups 1 and 3, respectively. Sample W5 is the dissolved sulfate in the groundwater outflowing at the East wall of the Exótica open pit; the sample EX5 is the precipitated gypsum at that site (Fig. 1K). Samples of potential sulfate sources from sedimentary formation of the region (Cordillera de la Sal) include gypsum (sample CS1) and anhydrite (sample CS2)

et al. 2014). This confined neutral saline groundwater had very low copper concentration and SO_4/Cl ratio (0.13 mg/L and 0.16, respectively; confined groundwater sample CT-8, Smuda et al. 2014). The isotopic compositions of the sulfate in this sample ($\delta^{34}S$ 4.4‰, $\delta^{18}O$ 13.5‰; Smuda et al. 2014) suggest its origin from dissolution of sedimentary gypsum/anhydrite similar as those from the Cordillera de la Sal ($\delta^{34}S$ 3.1‰, $\delta^{18}O$ 8.4–10.4‰; Table 6 and $\delta^{18}O_{sulfate}$–$\delta^{34}S_{sulfate}$ plot in Fig. 8). Additionally, the δ^2H and $\delta^{18}O$ ratios of the water from CT-8 (−71.5‰ and −9.8‰, respectively) are within the range of the isotopic composition of the solutions associated with Exótica gels ($\delta^{18}O$ −7.6 to −3.8‰, δ^2H −72.7 to −60.4‰; Table 6). The gel waters showed isotopic values overlapping with the pore waters from the Talabre tailings impoundment at Chuquicamata ($\delta^{18}O$ −7.6 to −3.8‰, δ^2H −64.6 to −43.0‰; (Spangenberg et al. 2007)). The isotopically heaviest waters associated to the gels suggest evaporative isotopic enrichment or contribution of drainage waters discharged from higher areas (Andean High Cordillera), or both.

The changes in the SO_4/Cl ratios of the groundwaters and associated minerals provide information on the hydrological situation at the southern part of the Exótica open pit, where the Fortuna gravels grade into the succession typical for the Calama basin, during the 2009 sampling campaign (Fig. 9). In the transition of the Exótica valley to the Calama basin, erosional material from the oxidation zone of Chuquicamata was deposited in the upper Calama Formation and most likely also in the Lasana and Jalquinche Formations (Fig. 9). The presence of oxide/exotic mineralization towards the south may explain the high copper concentrations in these

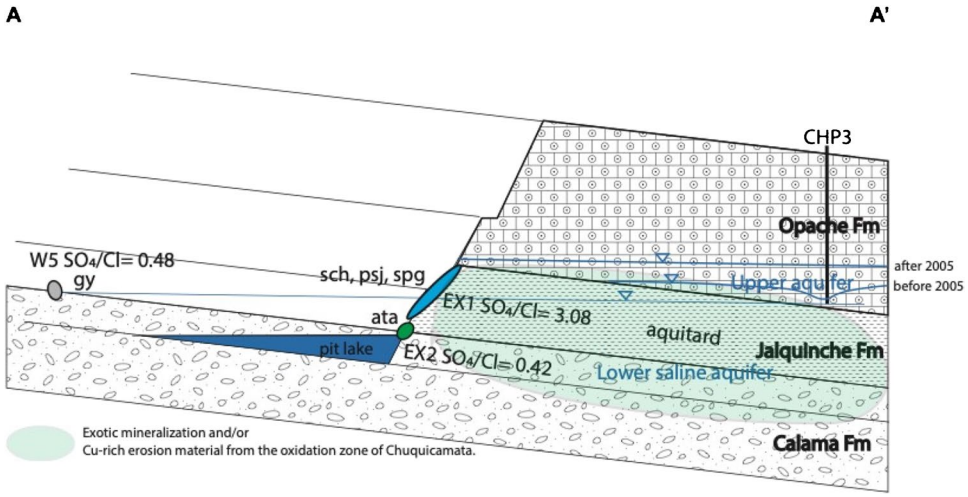

Fig. 9 Schematic N-S cross-section of the hydrogeological situation at the southern part of the Exótica open pit (site I) during the 2009 sampling campaign (section A-A' in Fig. 1). Abbreviations: ata, atacamite; gy, gypsum; psj, posnjakite; sch, schulenbergite; spg, spangolite

groundwaters (Fig. 9). The high Cl and NO_3 concentrations of the lower aquifer, as highlighted by some high saline outflows (W5 and EX2), suggest an evaporative stage at the final episode of sedimentation in the endorheic Calama Formation basin.

Finally, we discuss the effect of salinity and oxygen levels on dissolved copper speciation (i.e., Cu(I) and Cu(II) complexes) and mineralization at Exótica. In slightly reducing conditions, such as those encountered in a saline aquifer (< 500 mV), copper is in the form of Cu(I) chloride complexes ($CuCl_2^-$). This speciation of dissolved Cu was suggested by geochemical modeling of groundwater in the marine shore mine tailings deposit of Chañaral, Chile (Dold 2006). Oxidative conditions with Eh > 500 mV prevail in the outflow of the groundwater, resulting in the oxidation of Cu(I) to Cu (II) and formation of the $CuCl^+$ complex (Eq. 1). This copper chloride (+ 1) ion will hydrolyze to form atacamite with the liberation of 1.5 mol of H^+ per mole of $CuCl^+$ (Eq. 2). These reactions explain the drop of groundwater pH associated to the formation of atacamite in the outflow at the southern part of Exótica open pit (i.e., sample EX2).

$$CuCl_2^- - e^- = CuCl^+ + Cl^- \quad (1)$$

$$2CuCl^+ + 3\ H_2O = Cu_2(OH)_3Cl + Cl^- + 3H^+ \quad (2)$$

The copper source for the atacamite formation in the Chuquicamata-Exótica ore is assumed to be the dissolution of Cu-sulfates and hydroxides present in the Chuquicamata oxidation zone as a result of sulfide oxidation, as suggested from tailing studies (Dold and Spangenberg 2005; Smuda et al. 2014), which is also supported for example by the $\delta^{34}S$ value of − 2.1‰ of the brochantite sample EX3b (Table 6). In this case, the pH increased due to water–rock interactions in combination with the activities of sulfate and chloride in the solution along an evaporation-controlled flow path, triggering the precipitation of the atacamite/brochantite mineral assemblage.

Exotic mineralization and gels: is there a genetic link?

The mineralization of Exótica is composed predominantly of chrysocolla with locally co-precipitated Mn-oxides mainly birnessite, as well as Mn oxyhydroxides, partly as amorphous phases, known as copper pitch/wad (Dold et al. 2022). The morphology of banded ores in Exótica show similarities with that of the here described neoformed copper gels (Fig. 1A-H). The similarities in mineralogy, chemistry, and texture could suggest that part of the mineralization at Exótica formed initially from a similar gel-like material in surficial ponds fractures and porous materials. In order to discuss if the neoformed copper gels can represent present-day equivalents or precursors of the Exótica ore, the solutions leading to the formation of both precipitate types are reviewed in the following. In the neoformed gels, most copper sulfate hydroxides (e.g., spangolite, schulenbergite, posnjakite, and brochantite) precipitate from copper and sulfate-rich slightly acidic water (pH 6.0–6.5); the Cu-sulfate hydroxide devilline is stable in gels associated with near-neutral to slightly alkaline water (pH 7.2–7.8); atacamite precipitates from copper- and chloride-rich water with a pH slightly below 6.

As discussed by Dold et al. (2022) and explained in the four steps model summarized above, three types of ore-forming fluids were involved at the Exotica deposit. In step 1, supergene solutions were formed by sulfide oxidation from the adjacent Chuquicamata Cu-porphyry, resulting in acid rock drainage (pH 2–4) particularly rich in Cu, Si, and Mn. Starting from ARD with Cu^{2+} and SO_4^{2-} in solution, the

first mineral precipitating due to pH increase or Cu activity increase (e.g., through evaporation), or both, is chalcanthite (Jarrell 1944; Grevel and Majzlan 2011; Plumhoff et al. 2020). Under the hyper-arid conditions of the Atacama Desert, chalcanthite can dehydrate to bonattite (Dold and Fontboté 2001; Grevel and Majzlan 2011). At high copper activity or higher temperature, or both, antlerite is thermodynamically favored (Zittlau et al. 2013); at lower copper and sulfate activities, brochantite is favored (Jarrell 1944; Zittlau et al. 2013). These thermodynamic considerations explain why antlerite was only found as oxidation product in the chalcocite-enriched blanket of Chuquicamata, whereas in Exótica, brochantite was the only detected mineral associated with atacamite. If Ca^{2+} activity is high — due to gypsum and/or calcite dissolution — devilline can precipitate. The solubility of devilline is higher than that of the other copper minerals and is metastable with respect to brochantite and antlerite (Majzlan et al. 2015).

In steps 2 and 3, the acidic solutions were buffered by water–rock interaction (i.e., with Fortuna gravels consisting mainly of granodiorite) and/or by evaporation, which increased the activities of solutes in the solution/gels. This triggered the precipitation of chrysocolla and chrysocolla with co-precipitated Mn oxide and Mn oxyhydroxides (copper wad/pitch), forming the exotic deposit (Dold et al. 2022). The silicate weathering and kaolinization induced by the water–rock interaction released $H_3SiO_4^-$/$H_4SiO_4^\circ$ into solution, forming chrysocolla with Cu^{2+} above pH ~5. Laboratory studies have shown that Cu in solution prevents silica gel from precipitation and that concentrations of a few g/L dissolved silica form a hydrated copper-silica gel solution from which chrysocolla precipitates (Hariu et al. 2013). This synthetic chrysocolla had nearly identical XRD patterns to the Chuquicamata chrysocolla sample. Recently, it was shown that when the concentrations of Cu and Si increase during evaporation (Fernández-Mort et al. 2018), the activities decrease in the gel and prevent, for example, silica from precipitation. Due to the similarities in color and texture, it is generally accepted that the precursor of chrysocolla might also be a gel-like material (Newberg 1967; Tumiati et al. 2008; Hariu et al. 2013). Additionally, if ARD gets in contact with carbonates, georgeite, azurite, and malachite can precipitate (Pollard et al. 1991; Lytle et al. 2019). However, georgeite is rare as it is metastable with respect to malachite (Pollard et al. 1991) and mainly requires alkaline pH (Lytle et al. 2019). If the partial pressure of CO_2 is high enough, azurite is thermodynamically favored (Vink 1986; Kiseleva et al. 1992). Additionally, azurite requires more acidic conditions than malachite and can transform into it (Vink 1986; Crane et al. 2001; Melchiorre and Enders 2003; De Putter et al. 2010; Poot et al. 2020). Due to their different stability, azurite cannot be transformed into chrysocolla, while malachite can be replaced by chrysocolla (Vink 1986; Crane et al. 2001). These results provide a thermodynamically possible precipitation sequence when a Cu-rich ARD gets in contact with carbonate rocks and pH increases; precipitation of minerals starts with azurite, followed by malachite and, occasionally, georgeite under alkaline conditions. If subsequently, Si-rich solutions enter in contact with malachite, chrysocolla may replace malachite (Crane et al. 2001). At alkaline conditions, georgeite might be a bluish gel-like precursor of malachite (Pollard et al. 1991; Lytle et al. 2019).

In step 4, saline groundwater inflow resulted in an atacamite/brochantite mineral association on the top of the northern and central parts of the deposit impregnating cracks and pore spaces of the pre-existing chrysocolla — copper pitch/wad mineralization (Dold et al. 2022). If copper gets in contact with chloride-rich solutions, atacamite, paratacamite, and botallackite can precipitate (Pollard et al. 1989; Hannington 1993; Frost 2003; Malcherek et al. 2018). Upon contact with Cl-rich solution, copper sulfates like brochantite can transform into paratacamite. At high copper activity, atacamite is thermodynamically favored (Pollard et al. 1989). The formation and preservation of atacamite is favored in a system where an oxic copper deposit occurs in the presence of saline groundwater under hyper-arid conditions with extremely high evaporation rates. Such a situation applies to the hyper-arid region of northern Chile (Cameron et al. 2007; Reich et al. 2008, 2009; Fernández-Mort et al. 2018), whereas in similar oxic copper deposits elsewhere, atacamite is rare.

From this review of the fluids forming the Exótica deposit it can be concluded that only those slightly acidic or close to neutrality prevailing in step 4 are comparable to those found to form the neoformed gels. Finally, the question remains why atacamite/brochantite occurs in the late mineralization step 4 at Exótica and not the copper sulfate hydroxides (e.g., devilline, spangolite, schulenbergite, and posnjakite) found in present-day gels. An answer may be in the stability of the latter phases. Devilline is metastable with respect to brochantite and anglesite (Majzlan et al. 2015). Although no direct confirmation about the meta-stability of schulenbergite and spangolite could be found in the literature, the common association of these minerals with brochantite (Ohnishi et al. 2007; Biagioni et al. 2018) might suggest that they could also be metastable with respect to brochantite. Posnjakite was reported to act as a seed crystal for subsequent formation of brochantite and to be metastable with respect to brochantite (Krätschmer et al. 2002; Dabinett et al. 2008; Zittlau et al. 2013). Crystallization time, temperature, and probably also repeated dry-wet-dry cycles may have played an important role in subsequent re-dissolution and re-precipitation of the primary precipitates and their re-arrangement into more stable phases (Krätschmer et al. 2002). Therefore, in the oxidation zone of Chuquicamata and the Exótica deposits, the metastable main Cu-sulfate hydroxides in the

gels were transformed with time (maturation) mainly into brochantite. This mineralogical evolution is similar to the association of schwertmannite-jarosite-goethite-hematite in active porphyry copper tailings (Dold and Fontboté 2001; Dold 2003). During active oxidation of the copper ore, schwertmannite can be detected together with jarosite and goethite; however, schwertmannite could never be detected in old oxidation zones of porphyry copper ore deposits. Only jarosite, goethite, and hematite occur in oxidation zones because schwertmannite is metastable with respect to goethite (Childs et al. 1998).

Conclusions

The studied neoformed copper gels in the Exótica deposit south of the giant porphyry copper deposit of Chuquicamata contain trace amounts of atacamite and brochantite, minerals typical for step 4 at the Exótica deposit; however the gels are dominated by less common minerals such as devilline spangolite, schulenbergite, and posnjakite. The occurrence of a malachite crust below some gels is common. Chrysocolla, the main copper mineral of the mineralization at the Exótica deposit, was not identified in the studied copper gels. The mineralogical composition and the pH and the chemistry of the water-gel solutions sampled in-situ are intimately related. The Cu-hydroxide chloride atacamite precipitated from waters with high Cl activity and a pH slightly below 6. Most Cu-sulfate hydroxides (e.g., spangolite, schulenbergite, posnjakite, and brochantite) were associated with slightly acidic water (pH 6.0–6.5). In contrast, the Cu-sulfate hydroxide devilline is stable in gels associated with near-neutral to slightly alkaline water (pH 7.2–7.8). The latter received Ca^{2+} mainly from neutralization reactions of calcite and dissolution of gypsum. Slightly negative sulfur isotope values suggest that the sulfur source in the neoformed gels is primarily the oxidation of sulfides. Among the non-copper-bearing precipitates, gypsum precipitated first, then blödite (Na-Mg sulfate), and finally halite. Macroscopically, neoformed gels have similar textures as observed in the Exótica mineralization.

Similarities in mineralogy, chemistry, and texture suggest that part of the mineralization in the Exótica deposit formed initially from a similar gel-like material. It is proposed that gels in the Exótica deposit formed from acid rock drainage interactions and accumulated in surficial ponds, fractures, and porous materials and then matured to chrysocolla, Cu-pitch/wad from acid rock drainage. The obtained results support that atacamite and brochantite are linked to saline groundwater ingression (Dold et al. 2022).

Supplementary Information The online version contains supplementary material available at https://doi.org/10.1007/s00126-022-01148-6.

Acknowledgements We thank specially the CODELCO geology department (and a special thanks to José Rojas) for the support and help in this study. We also thank Prof. Juan Manuel Garcia Ruiz, University of Granada, Spain; Prof. Ray Frost, Queensland University of Technology, Australia; and Mireille Leboeuf and Prof. Massoud Dadras, CSEM SA, Neuchatel, Switzerland, for scientific and analytical support. We thank Prof. Broder Merkel (University of Freiberg, Germany) and Prof. Britta Planer-Friedrich (University of Bayreuth, Germany) for the help in the 2009 sampling campaign and the analysis of samples EX1 and EX2. Our gratitude is due to the collaborators from the F.-A. Forel Institute and University of Geneva, Switzerland: Sophie Michalet, Julien Meyer, Marie-Caroline Pinget, and from the University of Lausanne: Dr. Thierry Adatte, Dr. Pierre Von Lanthen, Prof. Hans-Rudolf Pfeifer, Jean-Claude Lavanchy, and Prof. Torsten Vennemann. We thank the anonymous reviewers for their comments and suggestions, which helped to improve this paper.

Funding Research financed by the Swiss National Science Foundation, Projects FNS 200021_129988 and 146484 and an Augustin Lombard grant of the SPHN Society of Geneva. Open access funding provided by University of Geneva

Declarations

Conflict of interest The authors declare no competing interests.

References

Almdal K, Dyre J, Hvidt S, Kramer O (1993) Towards a phenomenological definition of the term 'gel.' Polym Gels Networks 1:5–17

Bea SA, Ayora C, Carrera J, Saaltink MW, Dold B (2010) Geochemical and environmental controls on the genesis of efflorescent salts on coastal mine tailings deposits: a discussion based on reactive transport modeling. J Contam Hydrol 111:65–82

Biagioni C, Pasero M, Zaccarini F (2018) Tiberiobardiite, $Cu_9Al(SiO_3OH)_2(OH)_{12}(H_2O)_6(SO_4)_{1.5}\cdot$10H2O, a new mineral related to chalcophyllite from the Cretaio Cu prospect, Massa Marittima, Grosseto (Tuscany, Italy): occurrence and crystal structure. Minerals 8:152

Brimhall GH, Alpers CN, Cunningham AB (1985) Analysis of supergene ore-forming processes and groung-water solute transport using mass balance principles. Econ Geol 80:1227–1257

Cameron EM, Leybourne MI, Palacios C (2007) Atacamite in the oxide zone of copper deposits in northern Chile: involvement of deep formation waters? Miner Deposita 42:205–218

Carmona V, Pueyo JJ, Taberner C, Chong G, Thirlwall M (2000) Solute inputs in the Salar de Atacama (N Chile). J Geochem Explor 69–70:449–452

Childs CW, Inoue K, Mizota C (1998) Natural and anthropogenic schwertmannites from Towada-Hachimantai National Park, Honshu, Japan. Chem Geol 144:81–86

Crane MJ, Sharpe JL, Williams PA (2001) Formation of chrysocolla and secondary copper phosphates in the highly weathered supergene zones of some Australian deposits. Rec Aust Mus 53:49–56

Dabinett TR, Humberstone D, Leverett P, Williams PA (2008) Synthesis and stability of wroewolfeite, $Cu_4SO_4(OH)_6{\cdot}2H_2O$. Pure Appl Chem 80:1317–1323

De Putter T, Mees F, Decrée S, Dewaele S (2010) Malachite, an indicator of major Pliocene Cu remobilization in a karstic environment (Katanga, Democratic Republic of Congo). Ore Geol Rev 38:90–100

Dirección General de Aguas (2003) Determinación de los derechos de aprovechamiento de agua subterránea factibles de constituir en los sectores de Calama y llalqui, Cuenca del Rio Loa, II Region, Chile. Gobierno de Chile. Ministerio de Obras Publicas. Dirección General de Aguas. Departament de Administración de Recursos Hidricos, Santiago de Chile

Dold B, Fontboté L (2001) Element cycling and secondary mineralogy in porphyry copper tailings as a function of climate, primary mineralogy, and mineral processing. J Geochem Explor 74:3–55

Dold B (2003) Dissolution kinetics of schwertmannite and ferrihydrite in oxidized mine samples and their detection by differential X-ray diffraction (DXRD). Appl Geochem 18:1531–1540

Dold B, Spangenberg JE (2005) Sulfur speciation and stable isotope trends of water-soluble sulfates in mine tailings profiles. Environ Sci Technol 39:5650–5656

Dold B (2006) Element flows associated with marine shore mine tailings deposits. Environ Sci Technol 40:752–758

Dold B (2014) Evolution of acid mine drainage formation in sulphidic mine tailings. Minerals 4(2):621–641

Dold B, Pinget M-C, Fontboté F (2022) Genesis of the exotic chrysocolla – "copper pitch/wad" – atacamite/brochantite ore at the Exótica (Mina Sur) deposit, Chuquicamata, Chile. Miner Deposita. https://doi.org/10.1007/s00126-022-01147-7

Dušek K, Dušková-Smrčková M (2020) Volume phase transition in gels: its discovery and development. Gels 6:22

Enders MS, Knickerbocker C, Titley SR, Southam G (2006) The role of bacteria in the supergene environment of the Morenci Porphyry Copper Deposit, Greenlee County, Arizona. Econ Geol 101:59–70

Fennell T, Piatek JO, Stephenson RA, Nilsen GJ, Rønnow HM (2011) Spangolite: An s= 1/2 maple leaf lattice antiferromagnet? J Phys: Condens Matter 23:164201

Fernández-Mort A, Riquelme R, Alonso-Zarza AM, Campos E, Bissig T, Mpodozis C, Carretier S, Herrera C, Tapia M, Pizarro H, Muñoz S (2018) A genetic model based on evapoconcentration for sediment-hosted exotic-Cu mineralization in arid environments: the case of the El Tesoro Central copper deposit, Atacama Desert, Chile. Miner Deposita 53:775–795

Frost RL (2003) Raman spectroscopy of selected copper minerals of significance in corrosion. Spectrochim Acta Part A Mol Biomol Spectrosc 59:1195–1204

Graupner T, Kassahun A, Rammlmair D, Meima JA, Kock D, Furche M, Fiege A, Schippers A, Melcher F (2007) Formation of sequences of cemented layers and hardpans within sulfide-bearing mine tailings (mine district Freiberg, Germany). Appl Geochem 22:2486–2508

Grevel K-D, Majzlan J (2011) Internally consistent thermodynamic data for metal divalent sulphate hydrates. Chem Geol 286:301–306

Hannington MD (1993) The formation of atacamite during weathering of sulfides on the modern sea-floor. Can Mineral 31:945–956

Hariu T, Arima H, Sugiyama K (2013) The structure of hydrated copper-silicate gels, an analogue compound for natural chrysocolla. J Mineral Petrol Sci 108:111–115. https://doi.org/10.2465/jmps.121022c

Jarrell OW (1944) Oxidation at Chuquicamata, Chile. Econ Geol 39:251–286

Jordan T, Lameli CH, Kirk-Lawlor N, Godfrey L (2015) Architecture of the aquifers of the Calama Basin, Loa catchment basin, northern Chile. Geosphere 11:1438–1474

Kiseleva IA, Ogorodova LP, Melchakova LV, Bisengalieva MR, Becturganov NS (1992) Thermodynamic properties of copper carbonates — malachite $Cu_2(OH)_2CO_3$ and azurite $Cu_3(OH)_2(CO_3)_2$. Phys Chem Miner 19:322–333

Krätschmer A, Odnevall Wallinder I, Leygraf C (2002) The evolution of outdoor copper patina. Corros Sci 44:425–450

Kuksenok O, Deb D, Dayal P, Balazs AC (2014) Modeling chemoresponsive polymer gels. Annu Rev Chem Biomol Eng 5:35–54

Lytle DA, Wahman D, Schock MR, Nadagouda M, Harmon S, Webster K, Botkins J (2019) Georgeite: a rare copper mineral with important drinking water implications. Chem Eng J 355:1–10

Majzlan J, Zittlau AH, Grevel K-D, Schliesser J, Woodfield BF, Dachs E, Števko M, Chovan M, PlÁŠil J, Sejkora J, MilovskÁ S (2015) Thermodynamic properties and phase equilibria of the secondary copper minerals libethenite, olivenite, pseudomalachite, kröhnkite, cyanochroite, and devilline. Can Mineral 53:937–960

Majzlan J, Števko M, Chovan M, Luptáková J, Milovská S, Milovský R, Jeleň S, Sýkorová M, Pollok K, Göttlicher J, Kupka D (2018) Mineralogy and geochemistry of the copper-dominated neutral mine drainage at the Cu deposit Ľubietová-Podlipa (Slovakia). Appl Geochem 92:59–70

Majzlan J (2020) Processes of metastable-mineral formation in oxidation zones and mine waste. Mineral Mag 84:367–375

Malcherek T, Welch MD, Williams PA (2018) The atacamite family of minerals — a testbed for quantum spin liquids. Acta Crystallogr B 74:519–526

May G, Hartley AJ, Chong G, Stuart F, Turner P, Kape SJ (2005) Eocene to Pleistocene lithostratigraphy, chronostratigraphy and tectono-sedimentary evolution of the Calama Basin, northern Chile. Rev Geol Chile 32:33–58

Melchiorre EB, Enders MS (2003) Stable isotope geochemistry of copper carbonates at the Northwest Extension deposit, Morenci District, Arizona: implications for conditions of supergene oxidation and related mineralization. Econ Geol 98:607–621

Moreton S (2007) Copper-bearing silica gel from the walls of Tankardstown Mine, Co., Waterford Ireland. JAf Russell Soc 10:10–17

Mote TI, Becker TA, Renne P, Brimhall GH (2001) Chronology of exotic mineralization at El Salvador, Chile, by Ar-40/Ar-39 dating of copper wad and supergene alunite. Econ Geol 96:351–366

Münchmeyer C (1996) Exotic deposits-products of lateral migration of supergene solutions from porphyry copper deposits In: Camus F, Sillitoe RH, Petersen R (eds) Andean copper deposits: new discoveries, mineralization, styles and metallogeny. Soc Econ Geol, Spec Publ 16: 43–58

Murray J, Nordstrom DK, Dold B, Kirschbaum A (2021) Seasonal fluctuations and geochemical modeling of acid mine drainage in the semi-arid Puna region: the Pan de Azúcar Pb–Ag–Zn mine, Argentina. J S Am Earth Sci 109:103197

Newberg DW (1967) Geochemical implications of chrysocolla-bearing alluvial gravels. Econ Geol 62:932–956

Nordstrom DK, Blowes DW, Ptacek CJ (2015) Hydrogeochemistry and microbiology of mine drainage: an update. Appl Geochem 57:3–16

Ohnishi M, Kusachi I, Kobayashi S, Yamakawa J (2007) Mineral chemistry of schulenbergite and its Zn-dominant analogue from the Hirao mine, Osaka, Japan. J Mineral Petrol Sci 102:233–239. https://doi.org/10.2465/jmps.061130

Orlandi P, Bonaccorsi E (2009) Montetrisaite, a new hydroxy-hydrated copper sulfate species from Monte Trisa, Vicenza, Italy. Can Mineral 47:143–151

Ossandón G, Fréraut R, Gustafson LB, Lindsay D, Zentilli M (2001) Geology of the Chuquicamata mine: a progress report. Econ Geol 96:249–270

Palache C (1939) Antlerite. Am Miner 24:293–299

Parkhurst DL, Appelo CAJ (2013) Description of input and examples for PHREEQC version 3—a computer program for speciation, batch-reaction, one-dimensional transport, and inverse geochemical calculations. US Geol Surv Tech Methods 6(43):497

Pinget M-C (2016) Supergene enrichment and exotic mineralization at Chuquicamata, Chile. Sciences de la Terre. University of Geneva, Geneva, Ph.D. thesis, p182

Plumhoff AM, Plášil J, Dachs E, Benisek A, Sejkora J, Števko M, Rumsey MS, Majzlan J (2020) Thermodynamic properties, crystal structure and phase relations of pushcharovskite [$Cu(AsO_3OH)(H_2O) \cdot 0.5H_2O$], geminite [$Cu(AsO_3OH)(H_2O)$] and liroconite [$Cu_2Al(AsO_4)(OH)_4 \cdot 4H_2O$]. Eur J Mineral 32:285–304

Pollard A, Thomas R, Williams P (1989) Synthesis and stabilities of the basic copper(II) chlorides atacamite, paratacamite and botallackite. Mineral Mag 53:557–563

Pollard AM, Thomas RG, Williams PA, Just J, Bridge PJ (1991) The synthesis and composition of georgeite and its reactions to form other secondary copper(II) carbonates. Mineral Mag 55:163–166

Poot J, Verhaert M, Dekoninck A, Oummouch A, El Basbas A, Maacha L, Yans J (2020) Characterization of weathering processes of the giant copper deposit of Tizert (Igherm Inlier, Anti-Atlas, Morocco). Minerals 10:620

Rech JA, Quade J, Hart WS (2003) Isotopic evidence for the source of Ca and S in soil gypsum, anhydrite and calcite in the Atacama Desert, Chile. Geochim Cosmochim Acta 67:575–586

Reich M, Palacios C, Parada MA, Fehn U, Cameron EM, Leybourne MI, Zuniga A (2008) Atacamite formation by deep saline waters in copper deposits from the Atacama Desert, Chile: evidence from fluid inclusions, groundwater geochemistry, TEM, and Cl-36 data. Miner Deposita 43:663–675

Reich M, Palacios C, Vargas G, Luo SD, Cameron EM, Leybourne MI, Parada MA, Zuniga A, You CF (2009) Supergene enrichment of copper deposits since the onset of modern hyperaridity in the Atacama Desert, Chile. Miner Deposita 44:497–504

Riquelme R, Tapia M, Campos E, Mpodozis C, Carretier S, González R, Muñoz S, Fernández-Mort A, Sanchez C, Marquardt C (2018) Supergene and exotic Cu mineralization occur during periods of landscape stability in the Centinela Mining District, Atacama Desert. Basin Res 30:395–425

Rivera SL, Alcota H, Proffett J, Díaz J, Leiva G, Vergara M (2012) Update of the geologic setting and porphyry Cu-Mo deposits of the Chuquicamata District, northern Chile. In: Geology and genesis of major copper deposits and districts of the world: a tribute to Richard H Sillitoe. Soc Econ Geol Spec Publ 16:19–54

Rogovina LZ, Vasil'ev VG, Braudo EE (2008) Definition of the concept of polymer gel. Polymer Sci Series C 50:85–92. https://doi.org/10.1134/S1811238208010050

Sáez A, Cabrera L, Garcés M, Pvd B, Jensen A, Gimeno D (2012) The stratigraphic record of changing hyperaridity in the Atacama desert over the last 10Ma. Earth Planet Sci Lett 355–356:32–38

Scheuber E, Bogdanic T, Jensen A, Reutter K-J (1994) Tectonic development of the North Chilean Andes in relation to plate convergence and magmatism since the Jurassic. In: Reutter K-J, Scheuber E, Wigger PJ (eds) Tectonics of the Southern Central Andes: structure and evolution of an active continental margin. Springer, Berlin Heidelberg, Berlin, Heidelberg, pp 121–139

Sillitoe RH (2005) Supergene oxidized and enriched porphyry copper and related deposits. Economic Geology 100th Anniversary Volume, Society of Economic Geologists, Littleton, Colorado, 723–768

Smuda J, Dold B, Spangenberg JE, Friese K, Kobek MR, Bustos CA, Pfeifer H-R (2014) Element cycling during the transition from alkaline to acidic environment in an active porphyry copper tailings impoundment, Chuquicamata, Chile. Journal of Geochemical Exploration 140:23–40

Spangenberg JE, Dold B, Vogt M-L, Pfeifer H-R (2007) Stable hydrogen and oxygen isotope composition of waters from mine tailings in different climatic environments. Environ Sci Technol 41:1870–1876

Spangenberg JE, Lavrič JV, Meisser N, Serneels V (2010) Sulfur isotope analysis of cinnabar from Roman wall paintings by elemental analysis/isotope ratio mass spectrometry — tracking the origin of archaeological red pigments and their authenticity. Rapid Commun Mass Spectrom 24:2812–2816

Tumiati S, Godard G, Masciocchi N, Martin S, Monticelli D (2008) Environmental factors controlling the precipitation of Cu-bearing hydrotalcite-like compounds from mine waters. The case of the "Eve verda" spring (Aosta Valley, Italy). Eur J Mineral 20:73–94

Vink BW (1986) Stability relations of malachite and azurite. Mineral Mag 50:41–47

White W (2010) Secondary minerals in volcanic caves: data from Hawaii. J Cave Karst Stud 72:75–85. https://doi.org/10.4311/jcks2009es0080

Zittlau AH, Shi Q, Boerio-Goates J, Woodfield BF, Majzlan J (2013) Thermodynamics of the basic copper sulfates antlerite, posnjakite, and brochantite. Geochemistry 73:39–50